JOURNAL OF GEOPHYSICAL RESEARCH, VOL. 97, NO. B13, PAGES 19,683–19,715, DECEMBER 10, 1992

Oceanic Crustal Thickness From Seismic Measurements and Rare Earth Element Inversions

ROBERT S. WHITE, DAN M^cKENZIE, AND R. KEITH O'NIONS

Department of Earth Sciences, Cambridge University, Cambridge, England

Seismic refraction results show that the igneous section of oceanic crust averages 7.1±0.8 km thick away from anomalous regions such as fracture zones and hot-spots, with extremal bounds of 5.0–8.5 km. Rare earth element inversions of the melt distribution in the mantle source region suggest that sufficient melt is generated under normal oceanic spreading centers to produce an 8.3±1.5 km thick igneous crust. The difference between the thickness estimates from seismics and from rare earth element inversions is not significant given the uncertainties in the mantle source composition, though it is of the magnitude that would be expected if partial melt fractions of about 1% remain in the mantle and are not extracted to the overlying crust. The inferred igneous thickness increases to 10.3±1.7 km (seismic measurements) and 10.7±1.6 km (rare earth element inversions) where spreading centers intersect the regions of hotter than normal mantle surrounding mantle plumes. This is consistent with melt generation by decompression of the hotter mantle as it rises beneath spreading centers. Maximum inferred melt volumes are found on aseismic ridges directly above the central rising cores of mantle plumes, and average 20±1 and 18±1 km for seismic profiles and rare earth element inversions respectively. Both seismic measurements and rare earth element inversions show evidence for variable local crustal thinning beneath fracture zones, though some basalts recovered from fracture zones are indistinguishable geochemically from those generated on normal ridge segments away from fracture zones. This is consistent with a model where the melt generated beneath spreading ridges is redistributed to intrusive centers along the ridge axis, from where it may flow laterally along the axis at crustal or surface levels. The melt may sometimes flow into the bathymetric lows associated with fracture zones. Oceanic crust created at very slow-spreading ridges, and in regions adjacent to some continental margins where rifting was initially very slow, exhibits anomalously thin crust from seismic measurements and unusually small amounts of melt generation from rare earth element inversions. We attribute the decreased mantle melting on very slow-spreading ridges to the conductive heat loss that enables the mantle to cool as it rises beneath the rift.

INTRODUCTION

New oceanic crust is formed by decompression melting of mantle welling up beneath diverging plates at spreading centers. One of the triumphs of early marine geophysics was in demonstrating that oceanic crust is thinner than continental crust and that it exhibits the same basic structure everywhere. This was known before seafloor spreading was recognised and before it was understood that new igneous crust is generated at spreading centers. Petrologic investigations of oceanic basalts show a similar consistency of composition, characterised as normal mid-ocean ridge basalt (MORB).

The source composition and depth of melting of MORB have been debated over the years. Recently there has been a convergence of opinion, based principally on the major and minor element composition of MORB [*Klein and Langmuir*, 1987; *M^cKenzie and Bickle*, 1988], that magmas are produced at depths of 70 km or less beneath mid-ocean ridges. This view is consistent with *M^cKenzie and O'Nions*' [1991] results for the melt distribution with depth, based on the inversion of rare earth element concentrations in the basalts. The main purpose of this paper is to compare estimates of igneous crustal thickness beneath the oceans made and interpreted using modern seismic refraction methods with melt thicknesses inferred from the rare earth element inversions.

Compilations of oceanic crustal structure from seismic experiments (e.g., *Raitt* [1963]), subdivided the crust into three distinct layers which have formed the reference basis for results from oceanic profiles for nearly three decades (Table 1). *Raitt* [1963] showed that beneath a variable thickness of sediments (Layer 1) were two more layers (2 and 3) which together comprise the igneous section of the crust. Layer 2 exhibits a wide range of seismic velocities and is commonly identified as the extrusive basaltic lavas and dykes formed at the spreading center. Layer 3 is much thicker, including over two-thirds of the igneous crust and exhibits consistent seismic velocities. It probably consists primarily of intrusive gabbroic rocks. Other authors [e.g., *Shor et al.*, 1970; *Christensen and Salisbury*, 1975] have produced compilations of normal oceanic crust which differ little from Raitt's model (Table 1).

Crust with an anomalous thickness is known from several geological settings in oceanic basins, including fracture zones, seamounts, elevated regions surrounding hot spots, marginal basins and the extremely young crust under active spreading centers. Recent compilations of oceanic structure (Table 2) have sought to exclude results from anomalous regions and from profiles with gross lateral inhomogeneity or poor mantle ar-

Paper number 92JB01749.
0148-0227/92/92JB-01749$05.00

TABLE 1. Normal Oceanic Crustal Structure From Slope – Intercept Solutions

	V, km/s	H, km
Raitt [1963] (*Atlantic + Indian + Pacific, Seafloor > 3000 m*)		
Layer 2	5.07 ± 0.63	1.71 ± 0.75
Layer 3	6.69 ± 0.26	4.86 ± 1.42
Mantle	8.13 ± 0.24	
Igneous Crustal Thickness		6.57 ± 1.61
Shor et al. [1970] (*Pacific, seafloor > 2500 m*)		
Layer 2	5.19 ± 0.64	1.49 ± 0.98
Layer 3	6.81 ± 0.16	4.62 ± 1.30
Mantle	8.15 ± 0.30	
Igneous Crustal Thickness		6.11 ± 1.63
Christensen and Salisbury [1975] (*"Main" Basins, Age > 40 Ma*)		
Layer 2	5.04 ± 0.69	1.39 ± 0.50
Layer 3	6.73 ± 0.19	4.97 ± 1.25
Mantle	8.15 ± 0.31	
Igneous Crustal Thickness		6.36 ± 1.35

rivals. As compilers have become more selective there has been a tendency for the calculated mean crustal thickness to become smaller, with the most recent compilation, over normal crust with less than 0.5 km residual depth anomaly, giving a mean igneous thickness of only 5.84 km [*Keen et al.*, 1990]. We re-evaluate the information on oceanic crustal thickness from seismic refraction profiles and show that it is important not only to avoid known areas of anomalous structure, but also to ensure that the seismic data are interpreted by comparison with synthetic seismograms. The simpler travel time slope – intercept method of interpretation may significantly underestimate the true thickness.

The thickness of the igneous part of the oceanic crust may also be estimated from the melt distribution derived by inversion of rare earth element concentrations. The earliest and still some of the most accurate analyses of rare earth element concentrations were made by mass spectrometric isotope dilution [*Johnson*, 1979; *Sun et al.*, 1979; *Kay et al.*, 1970; *O'Nions and Grönvold*, 1973; *O'Nions et al.*, 1976]. Instrumental neutron activation analysis (INAA) has also been widely used to measure rare earth concentrations. Though the accuracy of older INAA measurements is often inferior, they are generally sufficient to obtain the melt distribution if the concentrations of seven or more rare earth elements were measured.

The inversion method used here is the same as that described by *McKenzie and O'Nions* [1991], with two differences. The first is that the top of the melting zone is taken to be at the base of the crust rather than at the

TABLE 2. Mean Crustal Thickness of Normal Oceanic Crust From Compilations of Slope – Intercept Solutions

Reference	Crustal Age, Ma	Number of Profiles	Mean Thickness, km	Comments
Hill [1957]	all	41	6.45 ± 1.92	Atlantic & Pacific, water >4000 m, excluding oceanic trenches.
Raitt [1963]	all	>126	6.57 ± 1.61	Atlantic, Indian & Pacific, water >3000 m, excluding deep trenches, continental slope, flanks of islands, oceanic rises.
Shor et al. [1970]	all	146	6.11 ± 1.63	Pacific only, water >2500 m, excluding trenches and outer ridges of trenches.
Christensen and Salisbury [1975]	>40	54	6.36 ± 1.35	'Main' basins excluding fracture zones, off ridge rises, plateaus and linear island chains.
Woollard [1975]	all	42	6.48	Pacific only, water >3000 m.
Houtz [1980]	all	26	5.59 ± 1.30	Atlantic only, Table 1 sonobuoys, excluding profiles with assumed mantle velocities, or mantle velocities <7.6 km/s.
McClain [1981]	all	99	5.83 ± 0.93	Pacific only, excluding fracture zones, seamounts, Hawaiian chain volcanics, grossly variable profiles.
McClain and Atallah [1986]	<30	44	5.67 ± 0.88	Pacific only, exclusions as *McClain* [1981].
	30–100	56	6.01 ± 0.91	
	all	100	5.86 ± 0.91	
Keen et al. [1990]	all	48	5.84 ± 1.12	Atlantic & Pacific, depth anomaly <0.5 km, excluding ocean islands, fracture zone traces, trenches, seamounts, marginal basins.

Earth's surface. The second concerns the melting path for the material in the melting zone. *McKenzie and O'Nions* [1991] assumed that all the melting occurred at the present depth of the residue, whereas it is more satisfactory to allow the melt to be generated at different depths as the mantle wells up. The expressions required to allow this are derived in Appendix A. *McKenzie and O'Nions* [1991] used two mantle compositions: depleted and primitive. The principal difference between them is in the concentrations of lanthanum and cerium. The choice of which composition is used for inversion has little effect on the calculated total melt thickness, though it does strongly affect how well the observed concentrations of lanthanum and cerium are reproduced, and hence the rms misfit.

McKenzie and O'Nions [1991] show that the crustal thickness calculated from inversions is sensitive to the absolute concentrations of rare earth elements assumed for the primitive Earth, decreasing by about 1 km when the concentrations are reduced by their estimated uncertainty of 10%. Hence the agreement between the seismic and geochemical estimates of the oceanic crustal thickness provides an independent check on the accuracy of *McKenzie and O'Nions*' estimated mantle composition.

Having determined the melt distribution with depth, it is straightforward to calculate the average major and minor element composition (Appendix B). The difference between the observed and calculated compositions is only significant at the 95% level if the relative misfit exceeds 2.

Data Compilation

We have taken care to construct a reference compilation from normal oceanic crust which can then be used as a standard against which to compare results from other settings. For both the seismic and the rare earth element data we have divided the observations into four classes: normal oceanic crust; anomalous oceanic crust (mainly very slow-spreading ridges and fracture zones); plume affected oceanic crust; and melt generated within rising mantle plumes.

Normal Oceanic Crust

The traditional slope – intercept method of interpreting seismic profiles was to make straight-line least-squares fits to the first arrivals and to invert them to a layered velocity-depth structure using the slopes and intercepts of the best-fitting lines [*Hill*, 1957; *Raitt*, 1963]. By the early 1980s sufficient computing power was available to model the seismic data either by finely layered structures to make more use of detailed variations in the travel time versus range information, or by comparison with synthetic seismograms to make use of the amplitude and waveform content.

The use of synthetic seismogram methods on oceanic profiles causes an increase of typically 20% over the thickness calculated by the slope – intercept method. This is apparent in Table 3 where we list results from 15 profiles over normal oceanic crust with a variety of ages, from both the Atlantic and the Pacific Oceans. For all the profiles the solutions published used first the slope – intercept and subsequently the synthetic seismogram interpretation method. In most cases the synthetic seismogram analysis of the same profile was made many years later by different workers, although in some cases both solutions were published by the same authors. In all cases except one (profile C16 for which no synthetic seismograms are illustrated by *McClain and Atallah* [1986], making it impossible to judge the goodness of the fit), the solution constrained by synthetic seismograms is thicker, by between 11% to 66%. This is true despite use of a large variety of synthetic seismogram techniques including reflectivity, WKBJ, generalised ray theory, Maslov, linearized travel-time inversion and automatic waveform inversion. Although we show results only from oceanic crust in Table 3, a similar increase in the thickness determined using synthetic seismogram methods is found in areas of anomalous crust such as active spreading centers [*Fowler*, 1976], aseismic ridges [*Sinha et al.*, 1981], fracture zones [*Potts et al.*, 1986*a*; *Whitmarsh and Calvert*, 1986], and ridges influenced by mantle plumes [*Bunch and Kennett*, 1980].

The main reason why slope – intercept solutions using a few homogeneous layers considerably underestimate the depth to the Moho is that the seismic velocity in oceanic crust increases relatively smoothly with depth as a series of gradients rather than in two or three uniform velocity layers. In the upper crust, the high velocity gradients are caused mainly by a downwards decrease in porosity as the cracks and fissures become closed [e.g., *Spudich and Orcutt*, 1980*b*]. In the lower crust the velocity gradients are much smaller (typically 0.1–0.2 /s compared to ~1.0 /s in the upper crust), and are probably caused by minor compositional or metamorphic changes and the effect of increasing pressure and temperature.

The first arrivals used by the slope – intercept method come mainly from rays which have turned in the upper part of the velocity gradient, because rays from deeper in the layer are masked as second arrivals. Since this apparent velocity is assumed to apply as a uniform value throughout the layer in the slope – intercept interpretation, adoption of too low an overall velocity results in calculation of too thin a layer from the travel times of returns from deeper horizons. This error is particularly marked for Layer 3, which comprises 70% of the crust.

This effect is illustrated in Figure 1 using a typical oceanic velocity structure derived from our compilation. We first ray-traced through the model using the velocity structure shown by the solid line in Figure 1. Three

TABLE 3. Difference Between Normal Oceanic Crustal Thicknesses Calculated Using Slope – Intercept and Synthetic Seismogram Methods

Profile		Thickness			Sources[a]
Identification	Age, Ma	Slope – Intercept, km	Synthetic Seismogram, km	Percentage Increase	
			Pacific Ocean		
CH-10	0–5	4.96	6.03	22%	*Shor et al.* [1970]; *Kennett and Orcutt* [1976]
C22	1	3.35	5.56	66%	*Shor et al.* [1970]; *McClain and Atallah* [1986]
C21	2	4.57	6.58	44%	*Shor et al.* [1970]; *McClain and Atallah* [1986]
C20	14	4.97	6.20	25%	*Raitt* [1956]; *McClain and Atallah* [1986]
C19	29	5.41	6.55	21%	*Raitt* [1956]; *McClain and Atallah* [1986]
C16	60	7.21	6.62	-8%	*Raitt* [1956]; *McClain and Atallah* [1986]
DW37	20	3.77	4.38	16%	*Shor et al.* [1970]; *Helmberger and Engen* [1978]
FF2	15	5.04	5.84	16%	*Shor et al.* [1970]; *Spudich and Orcutt* [1980*b*]; *Cary and Chapman* [1988]
FF4	15	5.94	6.84	15%	*Shor et al.* [1970]; *Spudich and Orcutt* [1980*b*]
			Atlantic Ocean		
Line A/SB1	56	5.33	6.29	18%	*Potts et al.* [1986*b*]
Line B/OBS3	54	4.13	5.06	23%	*Potts et al.* [1986*b*]
Line B/OBS4	54	4.09	5.14	26%	*Potts et al.* [1986*b*]
MAR 45N	3	5.02	6.83	36%	*Keen and Tramontini* [1970]; *Fowler and Keen* [1979]
10607/OBS6	3	5.64	6.25	11%	*Whitmarsh and Calvert* [1986]
10607/OBS7	8	5.98	6.96	16%	*Whitmarsh and Calvert* [1986]
Mean				23%	

[a]First named authors published the slope – intercept solution and second or subsequent authors published synthetic seismogram interpretation of the same profile. In cases where only one source is listed, the authors present both interpretations.

straight lines were then fitted by least-squares to the portions of the arrivals which appeared as first arrivals from the upper crust (layer 2), the lower crust (layer 3) and the mantle. The resultant slopes and intercepts of the straight line fits were then inverted, assuming that the crust consisted of uniform velocity layers. If the velocity and thickness of the sediment layer is known independently of the least-squares fit to layer 2 and 3 first arrivals, then the resultant two-layer igneous structure structure inferred from the slope – intercept solution (dashed line, *b*, Figure 1) has to be increased in thickness by 14% to match the true thickness. Most of the error lies in layer 3. However, if, as was often the case in older seismic profiles, the thickness of the sediment layer was not known but was instead calculated from the intercept of the underlying layer 2 arrival, then the inferred igneous crustal thickness from a two-layer slope – intercept solution to the first arrivals (dotted line, *c*, Figure 1), has to be increased by 19% to match the true thickness.

This result is typical of a large range of tests we have made using different water depths and a variety of detailed oceanic crustal structure curves. The error is typically 20%. It is striking that the mean of many separately published observations (Table 3) bears out this theoretical result.

In contrast, methods using synthetic seismograms can model the complex amplitude variations caused by interference with second arrivals. They can therefore detect velocity gradients in the crust, and can be used to distinguish between first-order discontinuities in velocity structure and gradational velocity changes within the crust. Although it is impossible to prove that any of the solutions is unique, it is clear that the models with velocity gradients are a better representation of the true velocity structure than are the older two-layered crustal models.

Seismic arrivals from the topmost crust may be masked by the high amplitude water wave [*White and Matthews*, 1980]. Some of the old measurements in the Pacific Ocean simply assumed that the 'hidden' layer was sedimentary [*McClain*, 1981]. In a few cases this is demonstrably wrong, and the igneous section should therefore be thicker than reported. The seismic velocity of the topmost basement may be as low as 2.1 km/s, particularly where it is very young and highly fractured [*Purdy*, 1987], so some layers which were previously thought to be sedimentary on the evidence of their low velocities (such as the 2.8 km/s layer recorded by *Fowler* [1976]) may in fact be igneous; this again means that the interpreted thickness of igneous crust from some older publications may be too small.

All the compilations listed in Table 2 make extensive, and often exclusive use of profiles interpreted using the slope – intercept method. However well they are filtered to remove anomalous regions they will al-

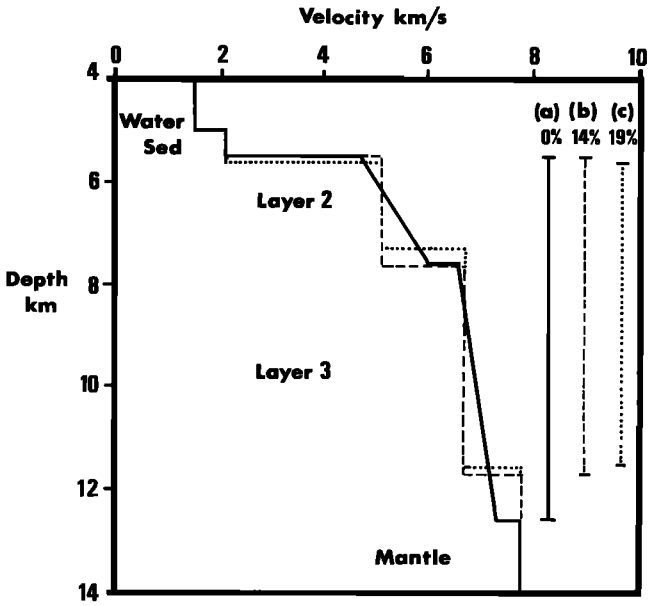

Fig. 1. The reduced crustal thicknesses inferred from two-layer slope – intercept interpretation of typical oceanic crustal structure. Solid line a shows typical oceanic velocity-depth structure derived from our velocity compilation. Dashed line b and dotted line c show the two-layer slope – intercept solutions derived from straight-line least squares fits to the first arrivals produced by a. Dashed line b shows inferred igneous thickness if the sediment velocity and thickness is known a priori. Dotted line c shows inferred thickness if the layer 2 intercept is used to calculate the overlying sediment thickness. Percentages are those by which the slope – intercept solutions have to be increased to match the true igneous thickness.

ways give incorrect crustal thicknesses because of the shortcomings of the interpretation method. We have therefore made a new compilation (Table 4) of the velocity structure of normal oceanic crust using only those profiles modeled by synthetic seismograms. No profiles have been included in our normal oceanic crust category from spreading ridges influenced by hot spots, from aseismic ridges above hot spots, from fracture zones, from marginal basins, or from spreading centers where normal mantle velocities above 7.6 km/s are not observed.

Our over-riding selection criterion has been to exclude any seismic profiles that exhibit residual basement depth anomalies with magnitudes in excess of 0.5 km. This removes profiles which may have thicker crust due to the occurrence of elevated mantle temperatures caused by a nearby mantle plume (e.g., Reykjanes Ridge profiles of *Bunch and Kennett* [1980]; Iceland Basin profiles of *Fowler et al.* [1989]; Azores-Biscay Rise profiles of *Whitmarsh et al.* [1982]; and profiles near the Hawaiian hot spot such as ESP 1 of *Lindwall* [1991] and SH31 of *Helmberger and Morris* [1970]). It also removes profiles which lie in areas that have been tectonically elevated, even though their crustal thicknesses may in fact remain normal (e.g., King's Trough profiles of *Searle and Whitmarsh* [1978]). Residual depth anomalies are found by backstripping the sediments [*Le Douran and Parsons*, 1982; *Renkin and Sclater*, 1988], and comparing the corrected basement depth with depth - age curves [*Parsons and Sclater*, 1977; *Hayes*, 1988]. Several profiles included in earlier compilations of results constrained by synthetic seismograms [*White*, 1984; *Spudich and Orcutt*, 1980*a*] are omitted because they do not satisfy our more stringent criteria. Our compilation for normal oceanic crust is listed in Table 4 and individual velocity-depth curves are shown in Figures 2 and 3.

For the geochemical inversion of normal MORB (Table 5) we use only analyses where the concentration of seven or more rare earth elements are reported on the same samples for which the concentrations of major and minor elements are available. We use only rocks with MgO $\geq$ 6%, for which we can calculate fractionation corrections with confidence from the Fe and Mg concentrations. This restriction also allows Eu to be used in the inversion, since its composition has not been affected appreciably by plagioclase separation in such magnesium-rich basalts. We do not exclude samples that contain appreciable amounts of water because rare earth element concentrations are little affected by hydrothermal alteration.

We attempted initially to identify the geochemical analyses from normal oceanic crust by their small local depth anomalies in the same way as we used for compiling the seismic results. However, this proved in detail to be an unsuccessful discriminant, although the average depth anomaly of all the locations of the geochemical samples from normal crust is indeed less than 0.5 km, as for the seismic determinations. It is not possible to use the local depth anomaly mainly because the depth from which an individual sample comes may not be representative of the regional depth anomaly: DSDP and ODP drill holes are often located in local sediment basins where it is easier to spud in, or where the sedimentary record is preserved, whilst dredges are usually taken up high scarps where there is most likelihood of basement outcrop. In addition, many of the best samples have come from close to the spreading centers, where the rocks are fresh. However, where spreading centers are still tectonically active, the local depth anomaly is not representative of the regional depth anomaly that the crust will exhibit when it moves out of the active zone. Lastly, there is the practical problem in many dredge hauls of great uncertainty in the original outcrop depth of individual samples.

For all these reasons, although we took note of the depth anomaly for our geochemical dataset, we also included any samples from active spreading centers that were not obviously affected by mantle plumes.

Anomalous Oceanic Crust

The most common source of anomalous crust in the oceans is fracture zones. There have been several detailed seismic surveys of fracture zones on the North

TABLE 4. Profiles Across Normal Oceanic Crust Modeled Using Synthetic Seismograms

Number	Identification	Age, Ma	Depth Anomaly[a], km	Igneous Crustal Thickness, km	Mantle Velocity, km/s	Source
			Pacific Ocean			
P1	ESP 1	0.2	-0.2	7.86[b]	7.9	*Vera et al.* [1990]
P2	Line 6W	0.5	-0.2	6.56	8.0	*Bratt and Solomon* [1984]
P3	Line 4	0.5	-0.1	6.57	8.0	*Bratt and Purdy* [1984]
P4	Line 4S	0.5	-0.2	6.60	7.9	*Lewis and Garmany* [1982]
P5	Line 5S	1	-0.2	6.40[b]	7.7	*Lewis and Garmany* [1982]
P6	Line 1S	1	-0.2	6.15	8.0	*Lewis and Garmany* [1982]
P7	C22	1	-0.5	5.56	7.8	*McClain and Atallah* [1986]
P8	C21	2	-0.1	6.58	7.6	*McClain and Atallah* [1986]
P9	66	2	0.0	5.60	8.1	*Lewis and Snydsman* [1979]
P10	B	3	0.1	8.10	7.6	*Orcutt et al.* [1976]
P11	OBS 1	4	0.0	7.38	8.0	*Waldron et al.* [1990]
P12	C	5	0.2	6.25	8.1	*Orcutt et al.* [1976]
P13	504B	6	-0.4	4.92	8.1	*Collins et al.* [1989]
P14	8	13	0.2	6.81	8.3	*Lewis and Snydsman* [1979]
P15	C20	14	0.0	6.20	8.1	*McClain and Atallah* [1986]
P16	FF2	15	0.1	5.83	7.8	*Cary and Chapman* [1988]
P17	FF4	15	0.2	6.67	7.9	*Spudich* [1979]
P18	C19	29	0.1	6.55[b]	7.6	*McClain and Atallah* [1986]
P19	C16	60	0.4	6.62	8.2	*McClain and Atallah* [1986]
P20	581C	115	0.1	7.28	8.2	*Duennebier et al.* [1987]
P21	Ngendei	140	0.4	6.70	8.2[c]	*Shearer and Orcutt* [1986]
			Atlantic Ocean			
A1	OBH 1	0	0.1	7.20	7.8	*Purdy and Detrick* [1986]
A2	Line E	1	-0.2	7.37	8.0	*Fowler* [1978]
A3	Lines A&B	2	0.4	7.72	7.9	*Fowler* [1976]
A4	MAR 45N	3	0.8	6.83	8.1	*Fowler and Keen* [1979]
A5	Line F	5	-0.3	6.25	7.9	*Fowler* [1978]
A6	10617	5	0.1	7.35	7.9	*Whitmarsh and Calvert* [1986]
A7	OBH 1	7	0.2	6.06	7.7	*Detrick and Purdy* [1980]
A8	9809	59	0.1	7.70	7.9	*Whitmarsh et al.* [1982]
A9	–	100	-0.1	7.05	(8.1)	*White* [1979]
A10	Line 1	110	-0.4	7.05	7.9	*Ginzburg et al.* [1985]
A11	Line 4W	124	-0.1	5.74[d]	8.0	*Whitmarsh et al.* [1990]
A12	ESP 5	125	0.2	7.92	8.0	*Cary and Chapman* [1988]
A13	Line 3	127	-0.4	6.81[d]	8.2	*Whitmarsh et al.* [1990]
A14	ESP 7In	142	0.2	7.80	8.0	*Minshull et al.* [1991]
A15	ESP 7Out	142	0.2	8.40	8.1	*Minshull et al.* [1991]
A16	ESP 8In	142	0.1	7.53	7.9	*Minshull et al.* [1991]
A17	ESP 8Out	142	0.1	8.03	8.3	*Minshull et al.* [1991]
A18	ESP 1In	143	0.1	7.35	8.0	*Minshull et al.* [1991]
A19	ESP 1Out	143	0.1	6.90	8.0	*Minshull et al.* [1991]
A20	ESP 2In	143	0.1	7.30	8.0	*Minshull et al.* [1991]
A21	ESP 2Out	143	0.1	7.30	8.0	*Minshull et al.* [1991]
A22	ESP 3In	143	0.3	7.70	7.9	*Minshull et al.* [1991]
A23	ESP 3Out	143	0.3	7.95	7.9	*Minshull et al.* [1991]
A24	ESP 13	143	0.1	7.10	8.2	*Minshull et al.* [1991]
A25	ESP 4In	143	0.3	7.38	8.1	*Minshull et al.* [1991]
A26	ESP 4Out	143	0.3	7.05	8.1	*Minshull et al.* [1991]
A27	ESP 15	144	0.1	8.04	8.2	*Morris et al.* [1992]
A28	–	144	0.3	7.45	(8.2)	*Purdy* [1983]
A29	ESP 16	146	-0.1	6.96	8.0	*Morris et al.* [1992]
A30	ESP 17	150	0.0	8.04	8.0	*Morris et al.* [1992]
A31	ESP 18	152	0.1	7.19	7.8	*Morris et al.* [1992]
A32	ESP 2	160	-0.2	8.44[b]	7.8	*Mithal and Mutter* [1989]
A33	ESP 4	170	-0.2	8.57[b]	7.6	*Mithal and Mutter* [1989]

[a]Depth anomaly calculated from difference between normal basement depth predicted from age of crust and measured depth after backstripping sediments. A positive depth anomaly means that corrected basement depth is shallower than predicted from its age. Only profiles with depth anomalies less than 0.5 km are included, with the exception of A4 which is over normal crust away from hot spots but is elevated because it lies on the crestal mountains adjacent to the Mid-Atlantic Ridge axis.

[b]Igneous crustal depth calculated to mid-point of Moho transition gradient. Value listed for mantle velocity is at mid-point of transition.

[c]Anisotropic mantle 7.95–8.40 km/s.

[d]Oceanic crust close to non-volcanic continental margin and therefore possibly anomalous (see Table 6).

Assumed mantle velocities in parentheses.

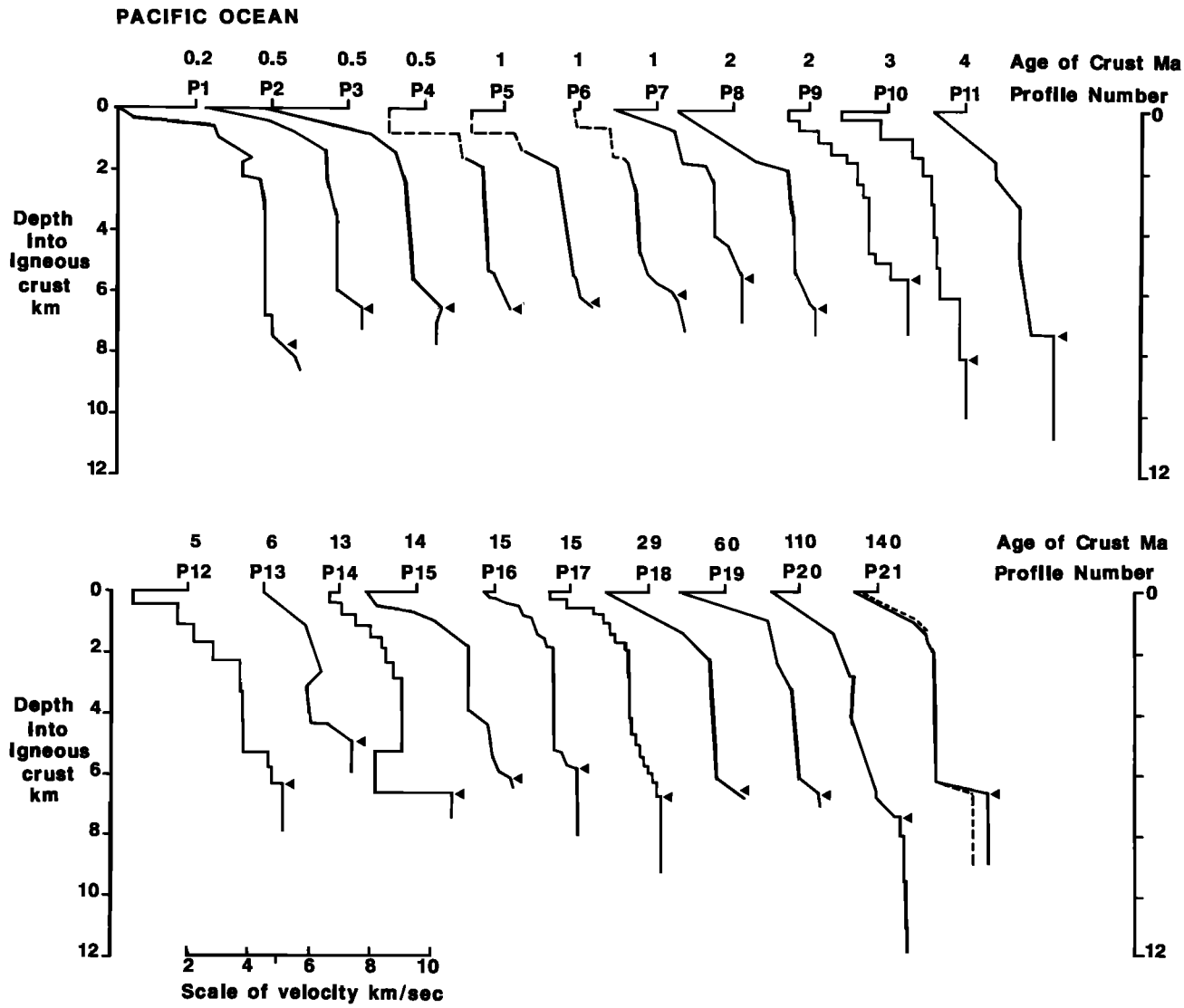

Fig. 2. Velocity-depth profiles of all available seismic profiles in the Pacific Ocean constrained by synthetic seismogram modeling from locations where the magnitude of the residual depth anomaly is less than 0.5 km. Sources are listed in Table 4. The profiles are aligned with zero depth at the top of the igneous basement. The horizontal scale of velocity is shown at the bottom of the figure, with the tick mark at the top of each profile aligned at 5 km/s. Arrowhead on each profile shows location of Moho. Broken lines show regions of uncertainty (as in profiles P4 and P5), or alternative interpretations presented by the original authors (as in profile P21, where there is seismic anisotropy in both crust and mantle on profiles at different azimuths in the same location).

Atlantic slow-spreading ridge (summarized by *White et al.* [1984] and *Minshull et al.* [1991]), but to date there have been few on fast-spreading ridges. In Table 6 we list all those results from fracture zones, including not only the few constrained by synthetic seismograms, but also those modeled using tau-sum or ray-tracing methods. Our experience is that results from the latter two methods are considerably improved over slope – intercept methods, and are generally close to interpretations using full waveform modeling [*Minshull et al.*, 1991].

Oceanic crust formed on very slow spreading ridges and adjacent to non-volcanic rifted continental margins is also anomalous in that it is often very thin. Few of the seismic profiles from these settings have been modeled using synthetic seismograms, although they are so thin that the anomaly is clear even from travel-time analysis. Reviews have been published by *Reid and Jackson* [1981], *Pinheiro et al.* [1992] and *White* [1992]: here we summarise the results in Table 6, but do not repeat the seismic velocity – depth curves.

Sites for geochemical analyses from fracture zones were also initially grouped on the basis of their geographic location. However, this classification was not satisfactory. Like *Bryan et al.* [1981], we found that the geochemistry of basalt samples from near the Kane fracture zone on the slowly spreading Mid-Atlantic ridge was indistinguishable from ridge axis samples. Similarly, basalts drilled from hole 522B in a South Atlantic fracture zone were the same as normal mid-ocean ridge basalts. The reason for this similarity may be that the

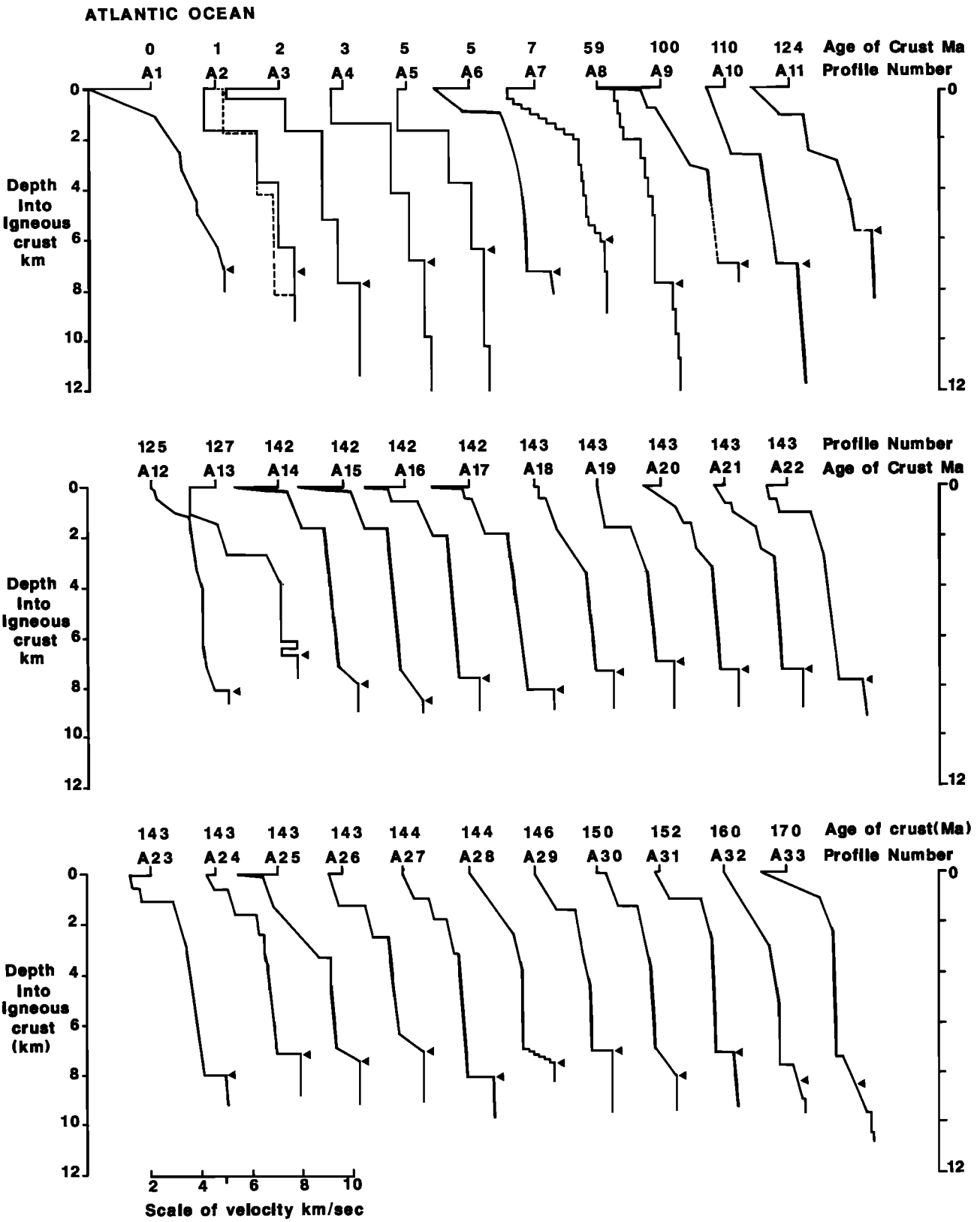

Fig. 3. Velocity-depth curves of all available seismic profiles in the Atlantic Ocean constrained by synthetic seismogram modeling from locations where the magnitude of the residual depth anomaly is less than 0.5 km. Sources are listed in Table 4 and annotation is the same as that described in the caption to Figure 2. Broken line on profile A2 shows alternative structure proposed by *Fowler* [1978]: Moho denoted by arrow on profile A2 and listed in Table 4 is the mean of the two alternatives presented by *Fowler* [1978]. Although the authors who originally published results of profiles A11 and A13 considered them to represent oceanic crust, and we have therefore included them here for completeness, recent work suggests that they may be anomalously thin because they lie close to non-volcanic continental margins (*White* [1992]; see also Table 6).

TABLE 5. Melt Thickness from Rare Earth Element Inversions

Identification[a]	Melt Thickness[b]			REE Misfit[c]	Source
	Before Fract., km	After Fract., km	Fract. Corr., %		
Normal Oceanic Crust					
R1 nr Kane FZ, N Atlantic	5.4	7.7	30	0.10	*Bryan et al.* [1981]
R2 Western N Atlantic	6.1	9.0	32	0.38	*Shimizu et al.* [1980]
R3 Central Atlantic	4.4	6.2	29	0.46	*Bougault et al.* [1988]; *Dosso et al.* [1991]
R4 Central Atlantic	6.0	7.9	24	0.16	*Rhodes et al.* [1979]
R5 South Atlantic	8.8	10.1	13	0.17	*Dietrich et al.* [1984]
R6 South Atlantic	6.6	8.2	20	0.14	*Dietrich et al.* [1984]
R7 East Pacific Rise	4.9	7.6	36	0.25	*Johnson* [1979]; *Sun et al.* [1979]; *Kay et al.* [1970]
R8 East Pacific Rise	3.7	5.9	38	0.12	*Thompson et al.* [1989]
R9 East Pacific Rise	6.8	8.7	21	0.34	*Bender et al.* [1984]
R10 East Pacific Rise	6.0	8.6	30	0.23	*Srivastava et al.* [1980]
R11 Mouth, Gulf of California	4.1	6.2	34	0.31	*Saunders* [1983]
R12 Eastern Pacific	6.4	9.7	34	0.26	*Pearce et al.* [1986]
R13 Costa Rica Rift	9.6	10.9	12	0.45	*Emmermann* [1985]
R14 Costa Rica Rift	8.5	11.0	23	0.16	*Tual et al.* [1985]
R15 Pigafetta Basin, Pacific	4.4	8.0	45	0.24	*Floyd et al.* [1992]
R16 S E Indian Ridge	8.0	8.4	4	0.24	*Klein et al.* [1991]
R17 S E & Central Indian Ridge	6.6	7.7	16	0.15	*Price et al.* [1986]
Mean Thickness	6.2±1.7	8.3±1.5			
Anomalous Oceanic Crust					
R18 Tamayo FZ, Pacific	2.2	3.2	30	0.21	*Bender et al.* [1984]
R19 Siqueros FZ, Pacific	0.8	1.5	47	0.57	*Srivastava et al.* [1980]
R20 Atlantis II FZ, East, SWIR	1.0	1.4	31	0.23	*Johnson and Dick* [1992]
R21 Atlantis II FZ, West, SWIR	1.4	2.0	29	0.16	*Johnson and Dick* [1992]
R22 E-MORB, East Pacific Rise	0.6	0.8	23	0.50	*Thompson et al.* [1989]
R23 S W Indian Ridge	4.8	4.8	–	0.39	*Price et al.* [1986]
R24 Mid-Cayman Rise	1.4	1.6	15	0.17	*Thompson et al.* [1980]
Mean Thickness	1.7±1.3	2.2±1.2			
Plume Affected Oceanic Crust					
R25 nr Azores, N Atlantic	11.0	11.8	6	0.68	*Wood et al.* [1979]
R26 nr Iceland, N Atlantic	6.1	10.0	39	0.42	*Wood et al.* [1979]
R27 Galapagos Rift	7.6	11.1	32	0.41	*Srivastava et al.* [1980]; *Emmermann et al.* [1983]
R28 nr Chagos-Laccadive Ridge	7.7	13.7	43	0.55	*Frey et al.* [1980]
Mean Thickness	8.1±1.8	10.7±1.6			
Melt Generated Within Plumes					
R29 Iceland basalts	12.2	17.9	32	0.27	*Grönvold* [1973]; *O'Nions and Grönvold* [1973]; *O'Nions et al.* [1976]
R30 Krafla	13.6	18.0	25	0.21	*Nicholson and Latin* [1992]
R31 Nauru Basin	11.1	18.5	40	0.71	*Saunders* [1985]
R32 Cret. volcs., Mariana Basin	13.0	19.2	32	0.67	*Floyd et al.* [1992]
R33 Ontong-Java Plateau	11.5	18.7	38	0.42	*Mahoney et al.* [1992]
Mean Thickness	12.3±1.0	18.5±0.5			
Anomalous MORB From Normal Ridge Axis					
R34 Central Atlantic near 14°N	8.7	10.3	16	0.30	*Bougault et al.* [1988]

REE inversions for R1–R24 and R27–R28 assume depleted mantle, for R25–R26 and R29–R34 assume primitive mantle.

[a]Identification numbers are the same as those used in the figures and in Table A1.

[b]Melt thickness shown in first column is calculated from rare earth element inversions; second column shows original thickness inferred after correction for the percentage shown in the third column that was fractionated out before basalts were emplaced.

[c]REE misfit is the root mean square value of [(observed-calculated)/standard deviation] for the rare earth elements.

TABLE 6. Seismic Profiles From Anomalous Oceanic Crust

Identification	Age, Ma	Depth Anomaly[a], km	Igneous Crustal Thickness, km[b]	Source
Oceanic Crust From Very Slow Spreading Ridges				
Arctic Line 3	~23	-0.1	2.7	*Jackson et al.* [1982]
Arctic Line 6	20	-0.2	1.5	*Jackson et al.* [1982]
Mean Thickness			2.1±0.6	
Oceanic Crust Near Non-Volcanic Rifted Margins				
Biscay 3, PUBS4	110	-0.3	5.8	*Ginzburg et al.* [1985]
Galicia 6	115	-0.1	4.3	*Horsefield* [1992]
Goban 3	100	0.3	5.4	*Horsefield et al.* [1992]
Iberia 3	127	-0.4	6.5	*Whitmarsh et al.* [1990]
Iberia 4W	124	-0.1	5.7	*Whitmarsh et al.* [1990]
Tagus 5	132	-0.3	1.8	*Pinheiro et al.* [1992]
Mean Thickness			4.9±1.5	
Fracture Zone Crust				
Blake-Spur ESP5Ain	142	0.1	4.0	*Minshull et al.* [1991]
Blake-Spur ESP5Aout	142	0.1	4.0	*Minshull et al.* [1991]
Blake-Spur ESP5out	142	-0.1	3.4	*Minshull et al.* [1991]
Blake-Spur ESP6in	142	-0.1	4.0	*Minshull et al.* [1991]
Blake-Spur ESP6out	142	-0.1	3.5	*Minshull et al.* [1991]
Charlie-Gibbs 10615	5.5	-1.0	3.5–5.0[c]	*Whitmarsh and Calvert* [1986]
Charlie-Gibbs 10617	5.4	-1.0	3.8[c]	*Whitmarsh and Calvert* [1986]
Fracture Zone I	~1	0.3	4.5[c]	*White et al.* [1984]
Kane Ex 1 OBH 7West	1	-1.1	6.7[d]	*Cormier et al.* [1984]
Kane Ex 1 OBH 8	3	-0.9	3.6[d]	*Cormier et al.* [1984]
Kane Ex 2 OBH 3	11	-1.4	2.8[d]	*Cormier et al.* [1984]
Kane Ex 2 OBH 3East	11	-1.4	2.6	*Cormier et al.* [1984]
Kane Ex 3 OBH 2	18	-0.2	3.2[d]	*Cormier et al.* [1984]
Kane Ex 3 OBH 2West	16	-0.3	3.5[d]	*Cormier et al.* [1984]
Oceanographer Line A(par.)	0–5	-0.3	4.2–5.5[c]	*Sinha and Louden* [1983]
Oceanographer Line A	3.8	-1.3	1.7[c]	*Sinha and Louden* [1983]
Oceanographer Line B	2	-1.0	4.3[c]	*Sinha and Louden* [1983]
Orozco Line 1, WH5-S & WH6-N	0.6	0.2	5.4	*Tréhu and Purdy* [1984]
Tydeman E1	69	0.3	2.8	*Potts et al.* [1986]
Tydeman OBS3	54	0.8	5.0	*Potts et al.* [1986]
Tydeman OBS4	56	0.9	5.2	*Potts et al.* [1986]
Vema Line A	0.5	-2.6	2.5[c]	*Potts et al.* [1986]
Vema Line B	2	-2.5	4.3[c]	*Potts et al.* [1986]
Vema Line C	0	-2.7	1.2[c]	*Louden et al.* [1986]
Vema FKI-E	0	-3.2	4.7[d]	*Detrick et al.* [1982]
Vema FKI-W	0	-3.2	6.0[d]	*Detrick et al.* [1982]
Vema JM2-W	0.5	-3.0	5.9[d]	*Detrick et al.* [1982]
Mean Thickness			4.0±1.3	

[a]Depth anomaly calculated from difference between normal basement depth predicted from age of the crust and measured depth after backstripping sediments. A positive depth anomaly means that the corrected basement depth is shallower than predicted from its age.

[b]Modeled using synthetic seismograms except as noted below.

[c]Modeled using ray-tracing methods.

[d]Modeled using tau-sum methods.

basalts sampled in the fracture zones flowed laterally into them from the adjacent ridge segments.

On the fast spreading East Pacific Rise two suites of samples from the Tamayo [*Bender et al.*, 1984] and Siqueiros [*Srivastava et al.*, 1980] fracture zones clearly differ in composition from those of most ridge axes suites. They resemble the composition of E-type MORBs from the East Pacific Rise, which *Thompson et al.* [1989] separated from other ridge axis basalts on the basis of their composition alone. They also resemble the composition of basalts from the very slowly spreading southwest Indian Ridge [*Price et al.*, 1986], and from

the Mid-Cayman Rise [*Thompson et al.*, 1980 and G. Thompson, personal communication, 1991], a 100 km long ridge segment on a 3000 km long transform fault. These five geochemical suites are therefore discussed together under the heading of anomalous oceanic crust, together with two suites from the Atlantis II fracture zone [*Johnson and Dick*, 1992].

Plume Affected Oceanic Crust

In this category we include crust formed at a spreading center which traversed the large region of unusually hot mantle surrounding a mantle plume. All 12 seismic profiles come from the vicinity of the Iceland plume in the North Atlantic, and all exhibit residual depth anomalies in excess of 0.5 km (Table 7).

Four suites of geochemical analyses come from this setting, one from near the Iceland plume at 63°N, one from near the Azores plume at 36°N, one from the Galapagos Rift and one from near the Chagos-Laccadive Ridge in the north-west Indian Ocean (Table 5).

Melt Generated Within a Mantle Plume

Mantle plumes lying beneath spreading centers generate very thick igneous crust. Seismic results controlled by synthetic seismogram modeling (Table 7) are currently available only from Kerguelen [*Recq et al.*, 1990], the Azores-Biscay Rise [*Whitmarsh et al.*, 1982], and the Madagascar Ridge [*Sinha et al.*, 1981], although simpler time – intercept determinations from other aseismic ridges such as the Iceland-Faeroes Ridge, the Chagos-Laccadive Ridge and the Ontong-Java Plateau also show very thick crust.

Geochemical inversions are shown from three suites of basalts generated within mantle plumes beneath Iceland and the Ontong-Java Plateau. Two other suites, from hole 462A in the Nauru basin [*Saunders*, 1985] and from hole 802A in the Mariana Basin [*Floyd et al.*, 1992] are also included. Although these magmas were emplaced 30 my or more after the oceanic basement was formed at these sites, they apparently represent massive lava flows from nearby mantle plumes. Their geochemistry is consistent with this origin.

One abnormal geochemical suite from the Mid-Atlantic Ridge at 14°N [from *Bougault et al.*, 1988] is shown separately as R34 in Table 5 . Inversion attempts for the melt distribution of this suite from the rare earth elements using a depleted mantle source identical to that used for normal, anomalous and plume affected oceanic crust could not reproduce the high concentrations of La and Ce present in the samples. However,

TABLE 7. Oceanic Seismic Profiles From Spreading Centers Affected By, and Above Mantle Plumes

Number	Identification	Age, Ma	Depth Anomaly[a], km	Igneous Crustal Thickness[b], km	Source
			Crust Affected by Iceland Plume		
H1	Line Z	9	1.6	9.9	*Bunch and Kennett* [1980]
H2	BI01	12	2.2	9.3	*Ritzert and Jacoby* [1985]
H3	BI02	15	1.9	7.9	*Ritzert and Jacoby* [1985]
H4	82-27	16	1.9	9.6[c]	*Larsen and Jakobsdóttir* [1988]
H5	OBS 4	50	1.9	10.8	*Morgan et al.* [1989]
H6	ESP 13	50	1.3	12.3[d]	*Mutter and Zehnder* [1988]
H7	ESP 19	50	2.0	6.9[d]	*Mutter and Zehnder* [1988]
H8	ESP 22	51	2.4	12.9[d]	*Mutter and Zehnder* [1988]
H9	ESP H	51	1.9	11.1	*Spence et al.* [1989]
H10	ESP G	52	1.7	11.2	*Fowler et al.* [1989]
H11	E46	54	0.7	10.4[d]	*Olafsson et al.* [1992]
H12	E45	56	0.9	11.7[d]	*Olafsson et al.* [1992]
Mean Thickness				10.3±1.7	
			Crust Generated Directly Above a Plume		
	Madagascar N-1	80	3.3	21.2	*Sinha et al.* [1981]
	Kerguelen 1	70	5.3	20.5	*Recq et al.* [1990]
	Kerguelen 2	70	5.3	18.5	*Recq et al.* [1990]
	S. Iceland	0–3	2.5	20–24[c]	Bjarnason et al. (submitted manuscript, 1992)
Mean Thickness				20.5±1.3	

[a]Depth anomaly calculated from difference between normal basement depth predicted from age of the crust and measured depth after backstripping sediments. A positive depth anomaly means that the corrected basement depth is shallower than predicted from its age.

[b]Modeled using synthetic seismograms except as noted below.

[c]Modeled using ray-tracing methods.

[d]Modeled using tau-sum travel time methods.

a satisfactory fit is obtained using a primitive upper mantle composition. The resulting crustal thickness of 10.3 km is 4 km thicker than that from adjacent parts of the Mid-Atlantic Ridge (R3). As *Bougault et al.* [1988] and *Dosso et al.* [1991] remark, the geochemistry of the basalts from this short section of ridge near 14°N resembles that of basalts from oceanic islands. There is, however, little evidence for any thermal anomaly associated with the geochemical differences, unlike all the other samples from plume-affected regions. The origin of this local geochemical anomaly is unclear, but is not obviously relevant to world wide melt production by ridges.

NORMAL OCEANIC CRUST

Determination of Crustal Thickness From Seismic Profiles

The Mohorovičić discontinuity (Moho) is commonly taken as the boundary between the crust and the mantle. There has in the past been much discussion and some confusion about various definitions of the Moho, with terms such as "seismic Moho", "reflection Moho", "petrological Moho", and even "gravity Moho" abounding (e.g., see discussion by *White* [1988]). The Moho was originally recognised using wide-angle seismic arrivals from the upper mantle, so we prefer to reserve the term "Moho" for the seismically determined depth to the upper mantle using wide-angle data such as that listed in Table 4.

The upper mantle exhibits an average velocity of 7.9–8.0 km/s, although under oceanic crust it displays horizontal anisotropy of up to 5% (e.g., profile P21), which contributes to scatter of measured velocities. Velocities in excess of 7.6 km/s are usually attributed to the mantle. A small positive velocity gradient is commonly found in the upper mantle. The Moho (arrowhead on velocity-depth curves in Figures 2 and 3) is chosen as the depth at which a normal mantle velocity structure first appears. In half the cases the Moho is a first-order discontinuity between lower crustal velocities of ~7 km/s and upper mantle velocities of >7.6 km/s and there is no ambiguity as to where it lies.

In the remaining cases the transition from crustal to mantle velocities is usually represented by a steep velocity gradient extending over a few hundred to a thousand meters. In these cases we have picked the Moho at the base of the transition zone. In five cases (denoted by superscript b in Table 4) where the upper mantle velocity structure has either not been defined well, or does not conform to the normal simple low velocity-gradient structure, we have assumed the Moho to be at the midpoint of the transition zone, provided the velocity at this depth is in excess of 7.6 km/s.

The seismically determined thickness from the top of the basement to the Moho is not necessarily identical to the igneous crustal thickness, but we contend that it is the same to within a few tens to a few hundred meters. The uncertainty arises from the geological structure in the vicinity of the Moho. In ophiolites the transition from crust to mantle is sometimes abrupt, and sometimes transitional over depths of up to a kilometer: this is similar to the range of velocity structures we find from seismic studies, with half exhibiting first-order velocity jumps and half displaying velocity gradients.

In ophiolites the transitional Moho zone is sometimes produced by an interfingering of ultramafics and mafic sills: such behaviour would produce velocity gradients similar to those we find in half the seismic profiles and by picking the Moho at the base of the transition zone we may overestimate the mafic crustal thickness by ~100–200 m from our seismic profiles. However, dunite bodies ranging in thickness from a few tens to a few hundreds of meters are often found in ophiolites at the base of the crustal section and these would exhibit high seismic velocities and therefore be attributed to the mantle section on seismic velocity profiles. If the dunites are formed by fractionation from partial melts, in those cases we would probably underestimate the igneous crustal thickness by a similar amount from our seismic profiles. So, on average, these two causes of uncertainty are likely to cancel out.

The base of the crust is often a structural as well as a petrological boundary. In the Bay of Islands ophiolite there is evidence of faulting along the base of the crust and in seismic reflection profiles there is strong evidence that the pervasive normal faults formed on the flanks of spreading centers often sole out near the Moho [*White et al.*, 1990]. In such cases the crust may be thinned slightly compared to its original thickness. Finally, the velocity gradient inferred in Moho transition zones from seismic data may sometimes be an artifact of the seismic inversion method. The assumption of lateral homogeneity implicit in most synthetic seismogram modeling methods employed in the studies reported here has the effect of producing an apparent velocity gradient zone from regions where an interface varies gently in depth: some of the apparent Moho transition zones recorded in Figures 2 and 3 may in practice be caused by lateral variations in the depth to the Moho.

The uncertainties in original crustal thickness caused by the factors discussed above are only small, of the order of a few hundred meters at most, and are far less than the variability between different profiles recorded in this compilation. They also act in both directions, sometimes causing our estimates to be too thin and sometimes too thick. We therefore contend that our compilation of depths to Moho is a good dataset with which to investigate oceanic igneous crustal thicknesses, and that the uncertainties are considerably smaller than the scatter between profiles.

The mean igneous crustal thickness of normal oceanic crust (omitting A11 and A13 which lie adjacent to non-volcanic continental margins) is 7.1±0.8 km. The thickness determinations fall in a tight distribution (Figure 4) with a mean 1.2 km greater than that of

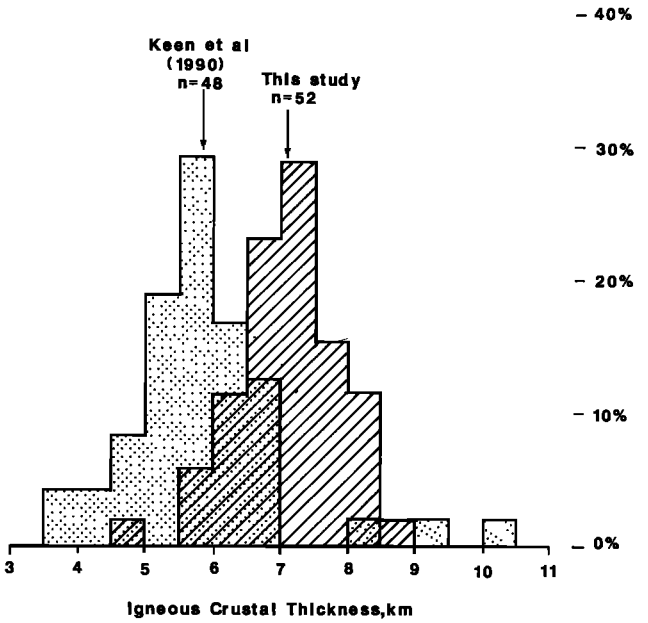

Fig. 4. Diagonally shaded histogram shows distribution of igneous crustal thickness from all oceanic seismic profiles constrained by synthetic seismogram modeling in locations where the magnitude of the residual depth anomaly is less than 0.5 km (this study, Table 4, excluding anomalous crust from A11 and A13 near non-volcanic continental margins). Lightly stippled histogram, for comparison, is compilation of thicknesses presented by *Keen et al.* [1990] of all oceanic profiles in locations with residual depth anomalies smaller than 0.5 km, but including a majority modeled only by travel time slope – intercept methods. The arrows show mean thicknesses from the two datasets.

the similar sized dataset from the Atlantic and Pacific Oceans reported by *Keen et al.* [1990]. The difference between our conclusions and those of Keen et al. and the other compilers listed in Table 2 can be attributed to the shortcomings of slope – intercept interpretations compared to more modern methods.

Oceanic Crustal Velocity-Depth Variation

When the velocity-depth variations from individual profiles are superimposed they give a remarkably consistent picture of the structure of normal oceanic crust (Figures 5 and 6). The uppermost 2 km (layer 2) exhibits large velocity gradients of the order of 1 /s. There is more scatter in the velocities from these shallow regions than from the lower crust, reflecting the variability in degree of fracturing, porosity and weathering which cause the low velocities in the upper crust [*Whitmarsh*, 1978]. The youngest crust exhibits the lowest seismic velocities in the topmost basement, reflecting the abundance of fissures, cracks and pore space which subsequently becomes filled by secondary weathering products to give increased velocities.

The lower crust (layer 3) exhibits far less scatter in velocities and much smaller velocity gradients. It is more than twice as thick as the overlying layer 2, and its onset can generally be located as an abrupt change to a lower gradient layer, frequently accompanied by a step in velocity to above 6.6 km/s. The velocity increases from typically 6.7 km/s at the top of layer 3 to about 7.2 km/s at the base. In some of the slope – intercept interpretations the higher velocity material at the base of the crust was interpreted as a separate layer 3B, although as our compilation makes clear there is very rarely any velocity jump in the middle of the lower crust: rather the velocity increases smoothly with depth as a result of the increase of pressure.

In Table 8 we show the mean crustal velocity structure from our compilation using conventional divisions into layers 2 and 3. This should be regarded as an updated version of the mean oceanic structures listed in Table 1.

Variation of Seismically Determined Crustal Thickness With Spreading Rate and Age

The crustal thickness varies relatively little at full spreading rates above 20 mm/yr, but apparently decreases markedly at lower spreading rates (Figure 7). Apart from two profiles on the very slow spreading Arctic Ridge [*Jackson et al.*, 1982], where the seafloor spreading tectonic framework is not well known, all the results from slow-spreading oceanic crust come from locations adjacent to non-volcanic rifted continental margins (Table 6). So it is important to ascertain whether the anomalously thin crust is a result of slow spreading or of proximity to a continental rift.

Recent results from the eastern Atlantic suggest that the effects of slow spreading can be separated from the effect of proximity to the continental margin. Profiles adjacent to the Goban Spur margin [*Horsefield et al.*, 1992] and in the Tagus abyssal plain [*Pinheiro et al.*, 1992] are across crust formed at a spreading rate of approximately 14–16 mm/yr, and show thin crust continuously over several tens of kilometers, from the continent-ocean boundary to as far oceanward as the profiles extend. This thin crust can thus be attributed to the slow spreading of the oceanic crust. In contrast, *Horsefield* [1992] has shown that profiles across the Galicia continental margin exhibit oceanic crust as thin as 4.3 km immediately adjacent to the ocean-continent boundary, but that within 15 km of the margin, the thickness has increased to that of normal oceanic crust. The spreading rate in this case was 22 mm/yr, so it appears that the first-formed crust was anomalously thin because it was derived from mantle which had risen initially beneath the stretching continent, but that as soon as the oceanic spreading center was fully developed, then normal thickness crust was formed. This again suggests that the critical spreading rate for the generation of normal thickness crust is around 20 mm/yr.

The explanation for thin crust under slow-spreading ridges is probably that the amount of melt produced by decompression in the rising mantle under the rifts is reduced by conductive heat loss from the mantle [*Reid and*

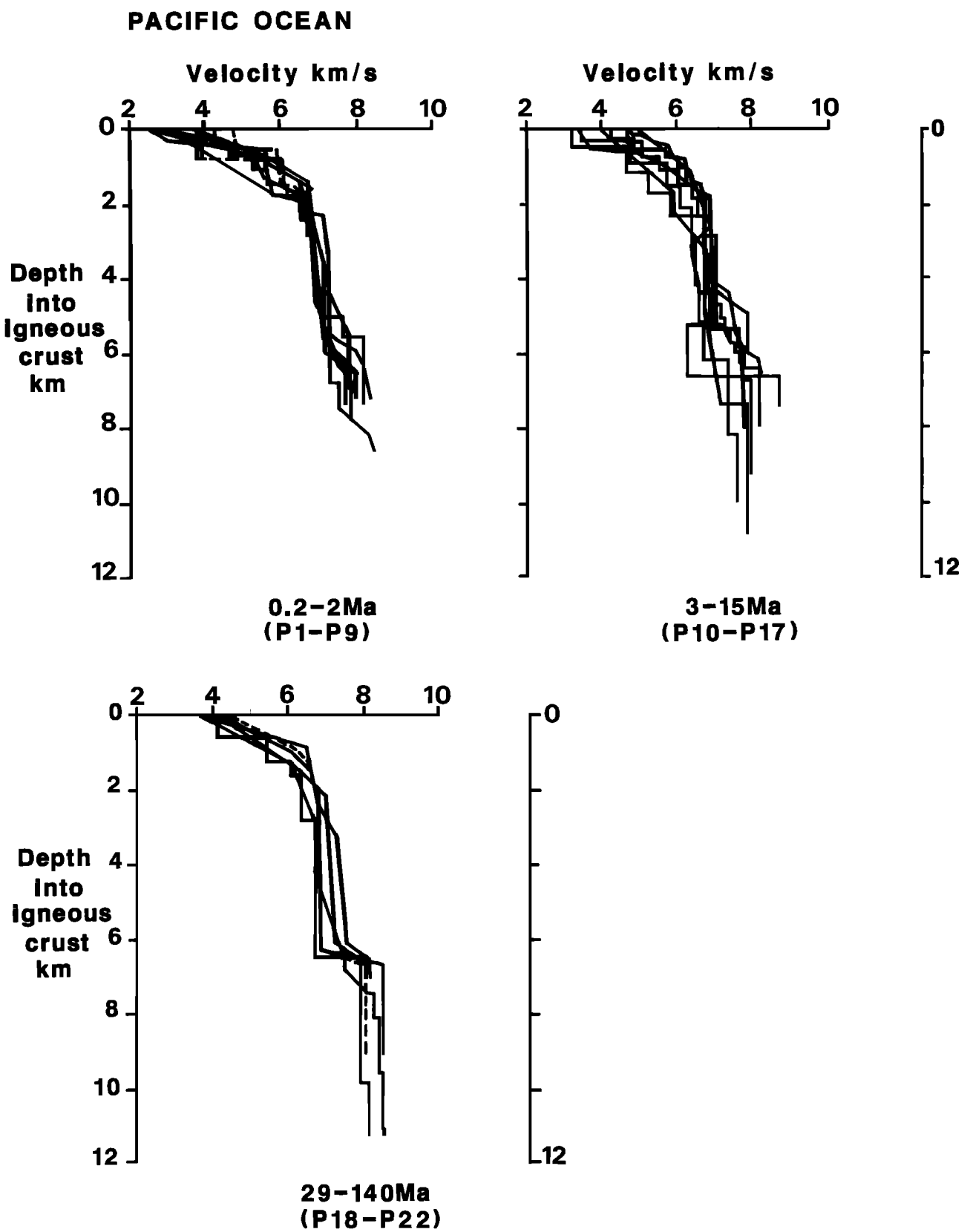

Fig. 5. Stacked velocity-depth curves for the profiles from the Pacific Ocean illustrated in Figure 2 and listed in Table 4.

Jackson, 1981]. In the oceanic crust immediately adjacent to non-volcanic continental margins, the oceanic spreading rate may not be unusually low once continental breakup has occurred, but there was often a long period of very slow stretching prior to breakup. Thus much of the mantle in the melt generation zone beneath the first-formed oceanic crust had already lost heat by conduction as it rose slowly beneath the stretching con-

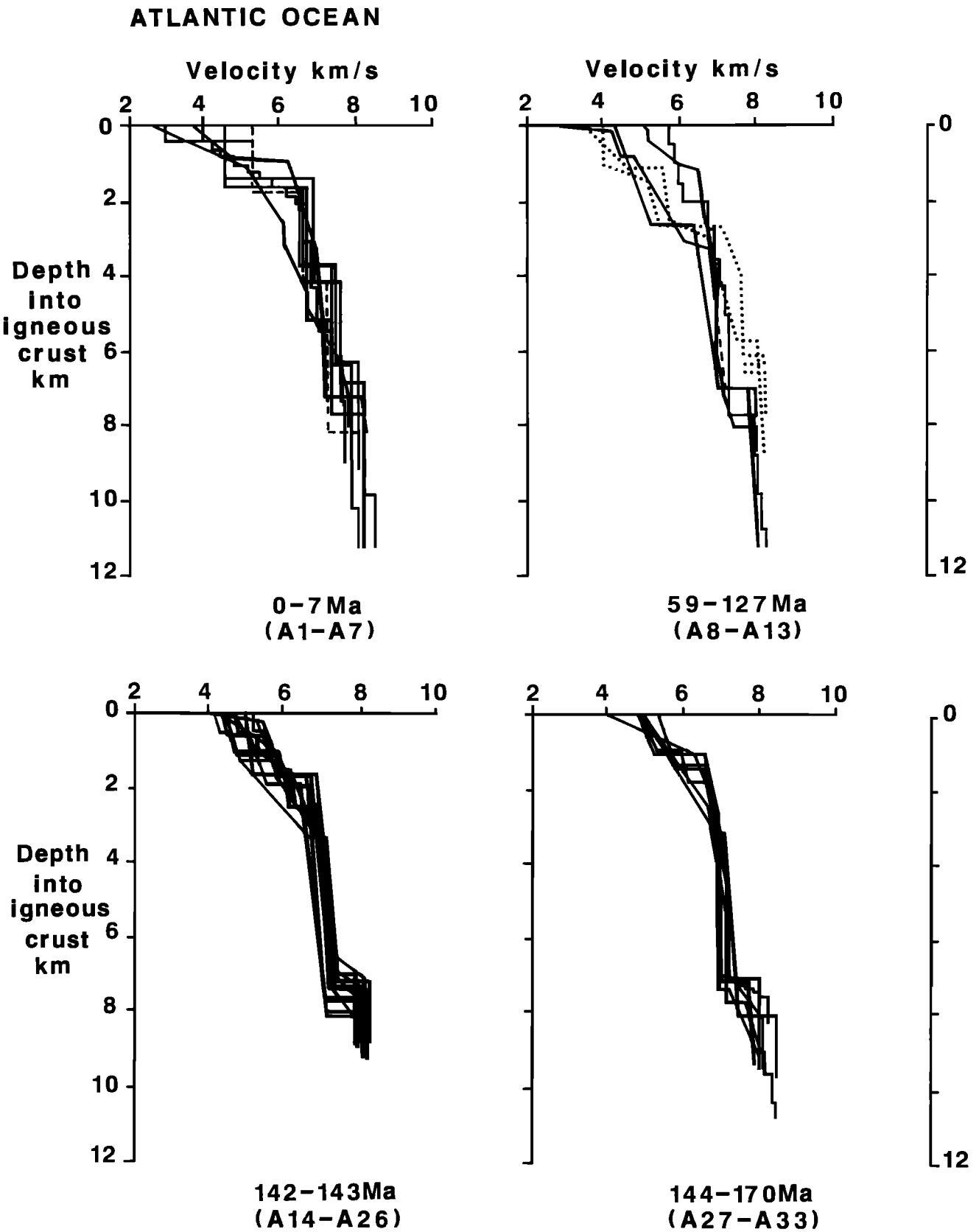

Fig. 6. Stacked velocity-depth curves for the profiles from the Atlantic Ocean illustrated in Figure 3 and listed in Table 4. Profiles A11 and A13 are shown dotted because although they are nominally just on the oceanic side of the ocean-continent boundary off Iberia [*Whitmarsh et al.*, 1990] they exhibit considerable lateral inhomogeneity and anomalous velocity structure which is not uncommon in this tectonic setting [*White*, 1992]: they are therefore probably not typical of normal mature oceanic crust.

TABLE 8. Normal Oceanic Crustal Structure From Profiles Modeled With Synthetic Seismograms (From Table 4, This Paper)

Location	Crustal Age, Ma	Number of Profiles	Mean Thickness, km
Pacific	< 30	18	6.48 ± 0.75
Pacific	> 30	3	6.87 ± 0.29
Atlantic	< 30	7	6.97 ± 0.57
Atlantic	> 30	24	7.59 ± 0.49
Atlantic and Pacific	all	52	7.08 ± 0.78

Mean Oceanic Crustal Structure (This Paper)

	Velocity, km/s	Thickness, km
Layer 2	2.5 – 6.6	2.11 ± 0.55
Layer 3	6.6 – 7.6	4.97 ± 0.90
Mantle	>7.6	
Total Igneous Crust		7.08 ± 0.78

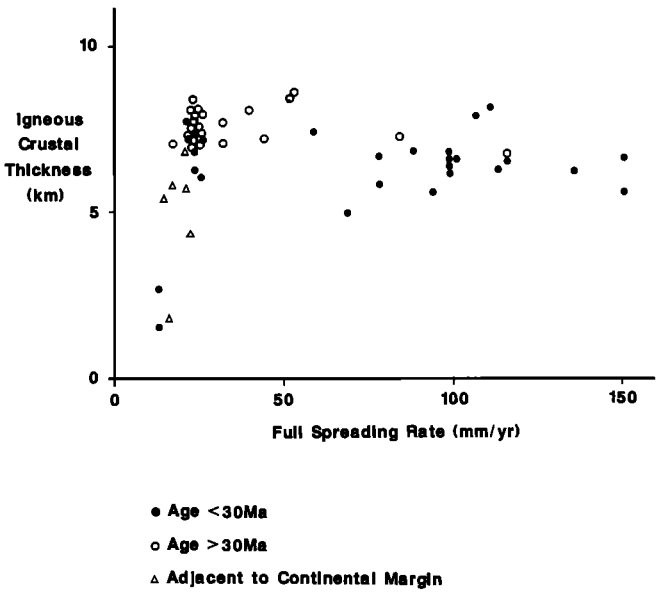

Fig. 7. Oceanic igneous crustal thickness as a function of spreading rate for all the profiles across normal oceanic crust (Table 4), and adjacent to non-volcanic rifted margins (Table 6), in locations where the magnitude of the residual depth anomaly is less than 0.5 km.

tinental lithosphere, and therefore the amount of melt produced may be reduced in exactly the same way as beneath the very slow-spreading ridges [*White*, 1992].

There is a suggestion in our dataset that the crustal thickness appears to increase slightly with age and that there is a tendency for thicknesses from the fast-spreading Pacific Ocean to be smaller than from the slow-spreading Atlantic Ocean (Table 8), although the variances are sufficiently large that the means are statistically indistinguishable. We also have very few well constrained measurements from older Pacific crust.

There have long been suggestions that the oceanic crust thickens with age [*Le Pichon et al.*, 1965; *Goslin et al.*, 1972; *Christensen and Salisbury*, 1975; *McClain*, 1981; *McClain and Atallah*, 1986], although as data from anomalous regions has been excluded, the magnitude of the allowable crustal thickening has decreased. *McClain and Atallah* [1986], using 100 seismic refraction profiles from the Pacific, suggest that the 30–100 Ma Pacific crust is some 0.34 km thicker on average than crust younger than 30 Ma (Table 2). Although these estimates were based mainly on thicknesses deduced from slope – intercept interpretations, they nevertheless provide a valid measure of the magnitude of crustal thickening because all the crustal determinations from both young and old crust are likely to be underestimated by a similar percentage. If we assume that the thicknesses used by *McClain and Atallah* [1986] are all about 20% too low, then the real crustal thickening is approximately 0.4 km.

We have insufficient seismic data over old crust in the Pacific Ocean to determine the presence of crustal thickening with age, though the mean values are consistent with *McClain and Atallah*'s [1986] result that the crust older than 30 Ma is about 0.4 km thicker than the crust younger than 30 Ma (Table 8). In the Atlantic Ocean, where there are far more synthetically modeled seismic profiles, which in addition extend over rather older crust, we find evidence for a similar degree of thickening, amounting to about 0.6 km (Table 8). All these results are consistent with about 0.4–0.5 km of thickening over a period of 100 my as the crust ages,

although in view of the sparse dataset, we are cautious about extending our conclusions any further.

On average the normal crust away from fracture zones on slow-spreading ridges appears to be about 0.5 km thicker than on fast-spreading ridges in the same age brackets (Table 8). We discuss later the evidence that this difference in thickness of normal ridge segments is caused by the greater density of fracture zones on slow-spreading ridges. We conclude that the overall thickness of the crust averaged across normal ridge segments and fracture zones is the same on both fast and slow-spreading ridges.

Melt Thickness From Rare Earth Element Inversions

The igneous thicknesses of normal MORB from the geochemical inversions (Table 5) average 8.3±1.5 km, in good agreement with that from seismics. Figure 8 shows the best fitting curve to each suite of rare earth elements, together with the resultant inferred distribution of melt fraction with depth.

The geochemical estimate of crustal thickness assumes that all the melt that is produced is removed to form crust. In practice a small melt fraction of perhaps 1% will remain behind, so the geochemical estimate of the amount of melt produced should be greater than the seismic measurements of the thickness of igneous rock that solidifies to form the crust. Though the mean seismic thickness is less than that from the rare earth element inversions, the difference of about 1 km is smaller than the likely uncertainty of the geochemical estimates. The spread of thickness determinations from seismic measurements is similar to the spread from geochemical estimates (Figure 9), giving confidence that the difference in the mean values is simply an offset due either to the retention of a small amount of melt in the mantle or to systematic error in the assumed primitive mantle rare earth element concentrations. *McKenzie and O'Nions* [1991] suggested that the uncertainty in their rare earth element concentrations in the primitive mantle was a maximum of 10%. If the primitive mantle source concentrations are reduced by this factor, the mean igneous thickness from rare earth element inversions is reduced to 7 km, and is then indistinguishable from the seismic estimate. It is therefore not clear whether the small difference between the seismic and the geochemical thickness estimates is real, as it could well be, or whether it is due to small errors in the geochemical assumptions.

Another test of the inversion scheme is the difference between the calculated and the observed major and minor element concentrations. In all 17 suites the only element for which this difference is significant is Mg (Appendix B). Loss of Mg is caused by olivine and pyroxene fractionation, and the mass lost in this way can be estimated from the calculated and observed Mg/Fe ratios [*McKenzie and O'Nions*, 1991]. Apart from this effect, which is well understood, the agreement between the calculated and observed concentrations is good.

In Figure 10 we show stacked curves of the inferred melt distribution with depth from all the rare earth inversions over normal oceanic crust (R1–R17). For comparison we superimpose a melting profile calculated using *McKenzie and Bickle*'s [1988] method with the assumption that the melting process is isentropic. Melting with a potential temperature of 1330°C generates a crustal thickness of 8.3 km, the same as the mean of the rare earth inversions. There is good agreement between the melt distribution inferred from the rare earth element concentrations, and those predicted by the forward modeling assuming decompression melting.

ANOMALOUS OCEANIC CRUST

Fracture Zones

It has been known for nearly a decade from seismic experiments that the crust beneath fracture zones is generally thinner than normal crust, typically being only half as thick but in places decreasing to as little as 1 km (Table 6 and Figure 11*b*). The thin crust extends over widths of around 10 km, although both the width and the thickness of fracture zone crust are very variable. It does not usually exhibit a normal layer 3 velocity despite the observation noted earlier that the seismic velocity in layer 3 is otherwise extremely consistent throughout the world's oceans. The explanation for this may be that unlike normal crustal sections where the lower crust is built up by multiple injections of melt from below, in fracture zones much of the melt may migrate laterally from the adjacent ridge sections and therefore undergo a quite different fractionation and solidification history. The pervasive faulting in fracture zones and the consequent deep penetration of water into the lower crust (which frequently leads to considerable serpentinisation of the underlying upper mantle) are also probably at least partially responsible for the anomalous lower crustal structure.

Rare earth inversions from fracture zone samples show varying results. On the slowly spreading South-West Indian Ridge the Atlantis II fracture zone (R20 and R21) shows crust only 1.4–2.0 km thick [*Johnson and Dick*, 1992], while samples from the Kane fracture zone and DSDP hole 522B in the Atlantic (R1 and R6) show normal crustal thickness. Two Pacific fracture zones (R18 and R19) show a marked reduction in melt generation with estimated igneous thicknesses of 3.2 and 1.5 km respectively. Since only a few suites are as yet available from fracture zones, this variability may be an artifact of sparse sampling. However, it is also likely that the near surface basalts sampled by drilling and by dredging have flowed laterally into the topographic low of the fracture zones from the adjacent ridge segments, so in those circumstances we would in any case expect frequently to see melt distributions appropriate for normal oceanic basalts from the geochemical inversions, although the deeper crust sampled by the seismic profiles may be anomalous.

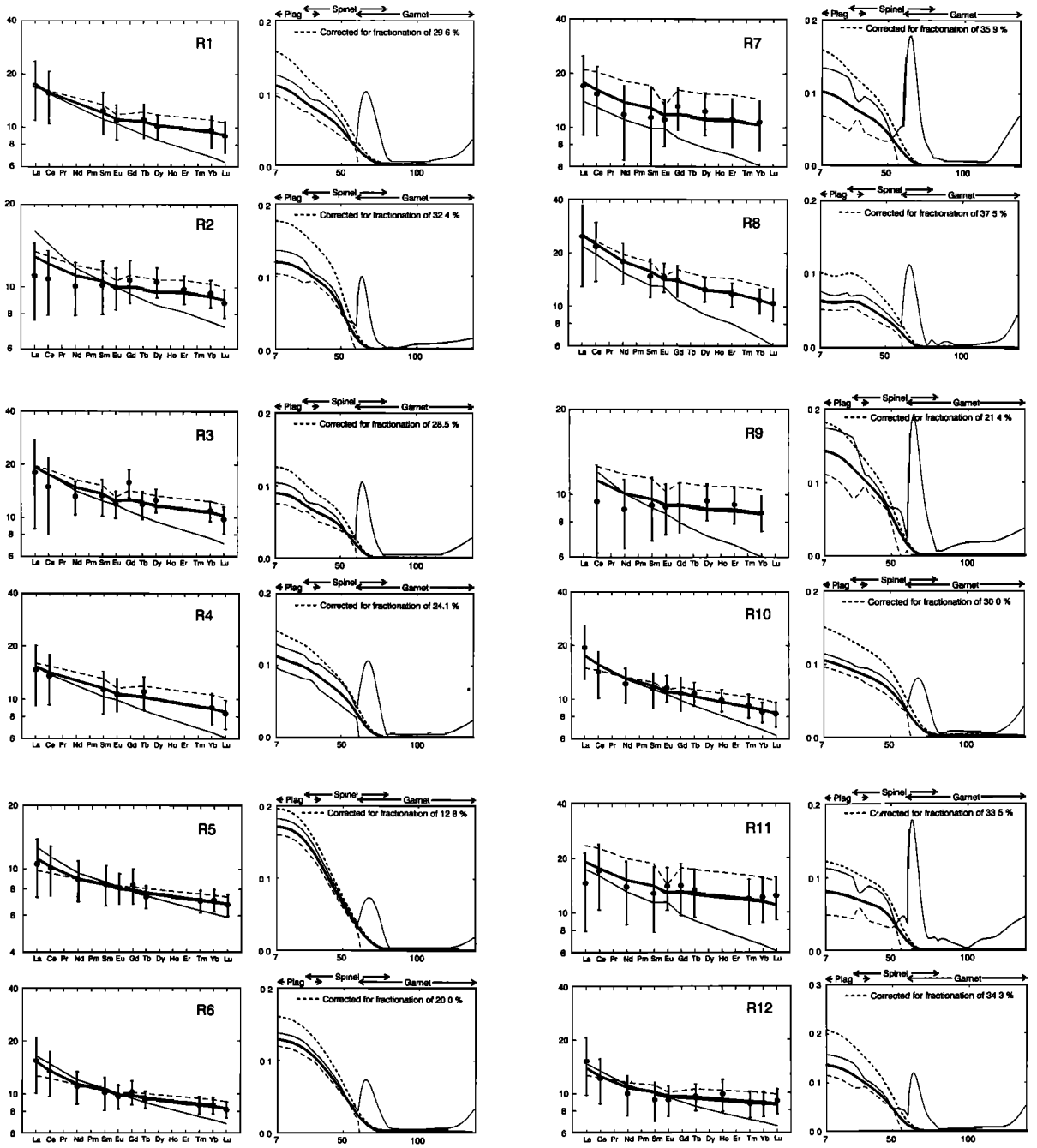

Fig. 8. Results of rare earth element inversions on the suites of basalts for samples R1–R34. For each sample, two graphs are illustrated. The left hand graph of the pair shows element concentration ratios, with heavy line showing the best fit to the data obtained by inversion. The fine continuous and dashed lines show the concentrations calculated from the estimated upper and lower bounds respectively to the melt fraction. The right hand graph of each pair shows the distribution of melt fraction by weight (vertical scale) with depth (horizontal scale) from inversion (solid line), and after correction for fractionation (short dashes). The top of the melting interval for suites R1–R17 and R34 is at an equivalent depth of 7 km, for suite R18 is at 30 km, for suites R19–R21 is at 40 km, for suite R22 is at 50 km, for suites R25–R28 is at 10 km, and for suites R29–R33 is at 16 km. These equivalent depths d assume that the overburden has the same density as the mantle, and are calculated from the melt thickness d_m and the water depth d_w using $d = 2.8d_m/3.3 + d_w/3.3$ with d_w approximated as 1 for normal and plume-affected crust and as 0 for crust built above mantle plumes. The bulk rare earth element concentrations used in the inversions were those for a depleted upper mantle for R1–R24 and R27–R28, and for a primitive upper mantle for R25–R26 and R29–R34. The estimated upper and lower bounds are shown as fine continuous and dashed lines respectively. The observed and calculated major element concentrations are shown in Appendix B. Sources of data and a summary of the inferred melt thickness and fractionation correction for each suite are listed in Table 5.

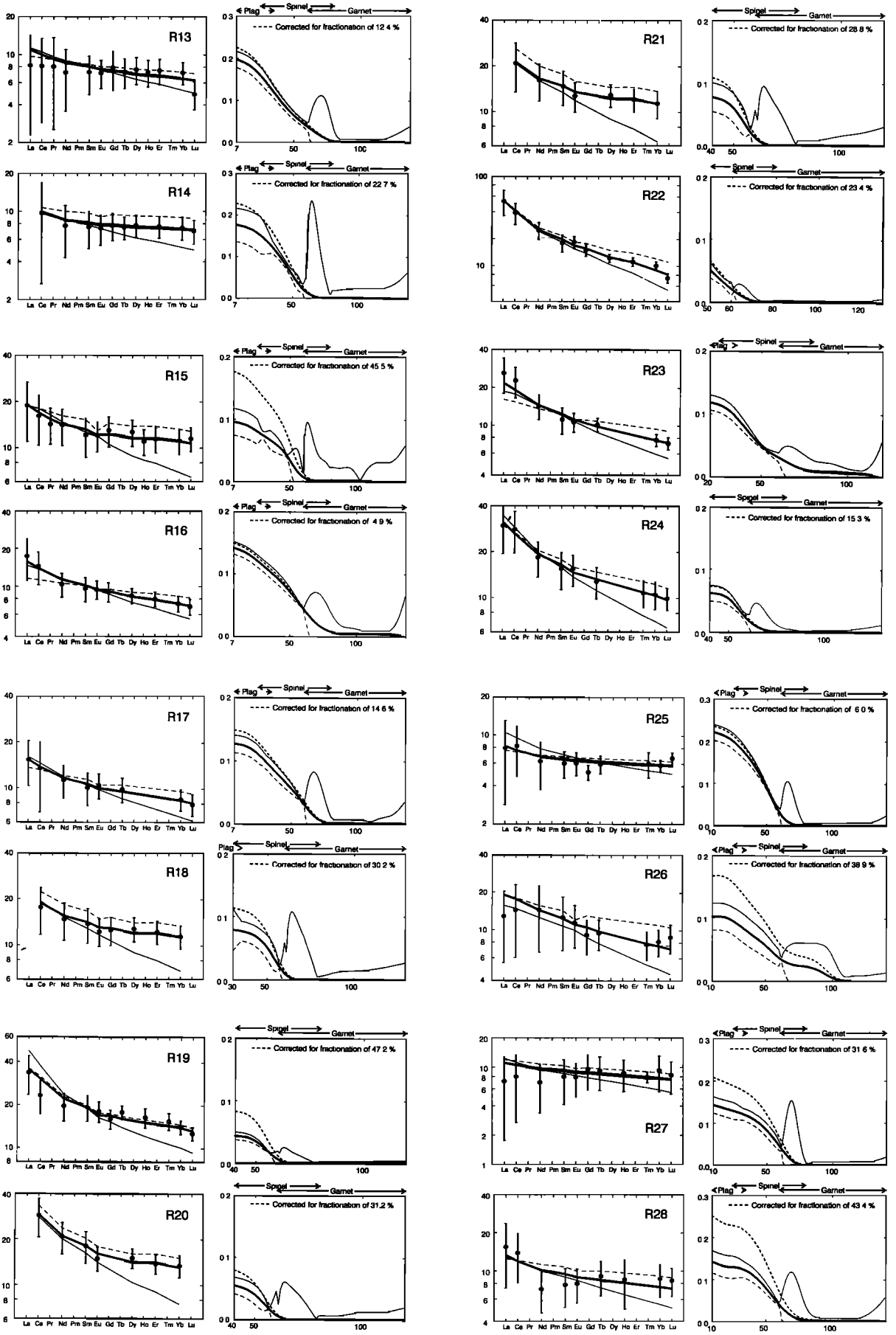

Fig. 8. (continued)

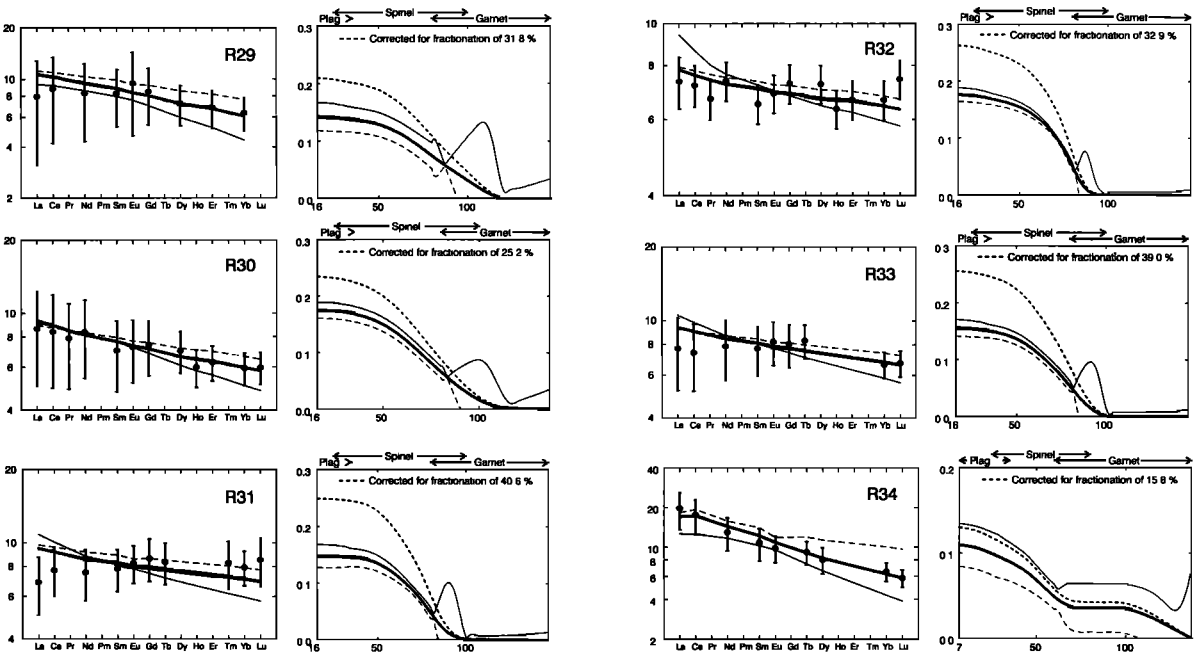

Fig. 8. (continued)

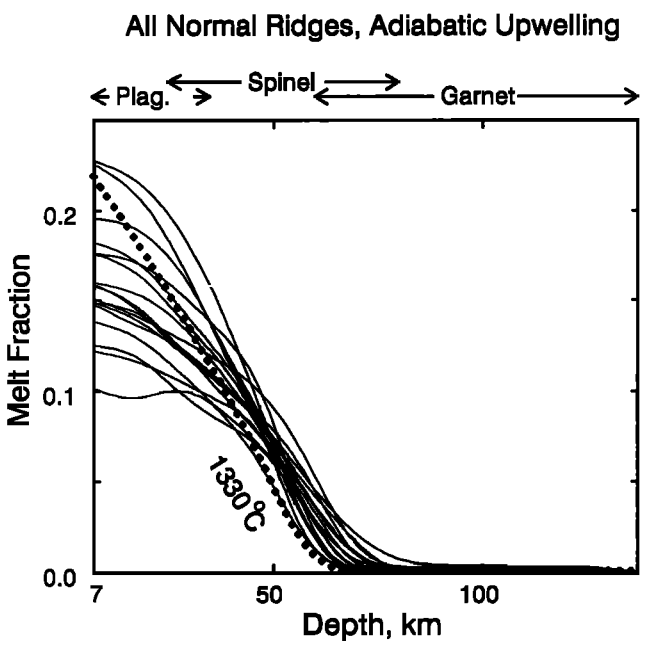

Fig. 9. Histograms of (a) seismic crustal thicknesses from normal oceanic crust listed in Table 4; (b) inferred melt thicknesses from rare earth element inversions on basalts from normal oceanic crust listed in Table 5; (c) map showing locations of seismic profiles and samples used to construct histograms. Open circles show sites of geochemical sampling, closed circles the locations of seismic profiles.

Very Slow Spreading Ridges

The thin crust indicated by seismic results from very slow-spreading ridges has already been discussed, when it was noted that oceanic crust generated adjacent to non-volcanic continental margins often exhibits similar thinning. A histogram of results from these environments is shown in Figure 11*a*.

Geochemical estimates of melt thickness from very slow-spreading ridges have been obtained from the Southwest Indian Ridge (R23), which has a spreading rate of only 14 mm/yr near its triple junction with the Central and Southeast Indian Ridges, and from the Mid-Cayman Rise (R24). Inferred melt thicknesses from these two suites are 4.8 and 1.6 km respectively. The rare earth inversions for R24 were first run with the top of the melting zone at a depth of 7 km, but the fits were poor. The depths were therefore increased for R24 to improve the agreement with the observed concentrations. The distributions of melt with depth for fracture zones and for very slow-spreading ridges are similar and are combined in the histograms of thicknesses shown in Figure 11*c* and in the stacked profiles in Figure 12.

Both seismic and the rare-earth element thickness determinations show anomalously small melt generation (Figure 11). This can be explained by conductive heat loss in the slowly rising mantle.

The origin of E-type MORB on the East Pacific rise is discussed by *Thompson et al.* [1989], and is not obviously associated with any tectonic process. As they point out, its eruption implies that some melt generated at the base of the melting zone must be able to reach the surface without mixing with that from shallower depths. The melt profiles obtained by inversion of these suites are all consistent with those for normal ridge axes and with the adiabatic profiles if no melt is generated above a depth of 30–50 km. As *Reid and Jackson*'s [1981] calculations show, this is the region that is most strongly affected by conductive heat loss.

In contrast to the rare earth element concentrations, the concentrations of SiO_2 and MgO calculated from

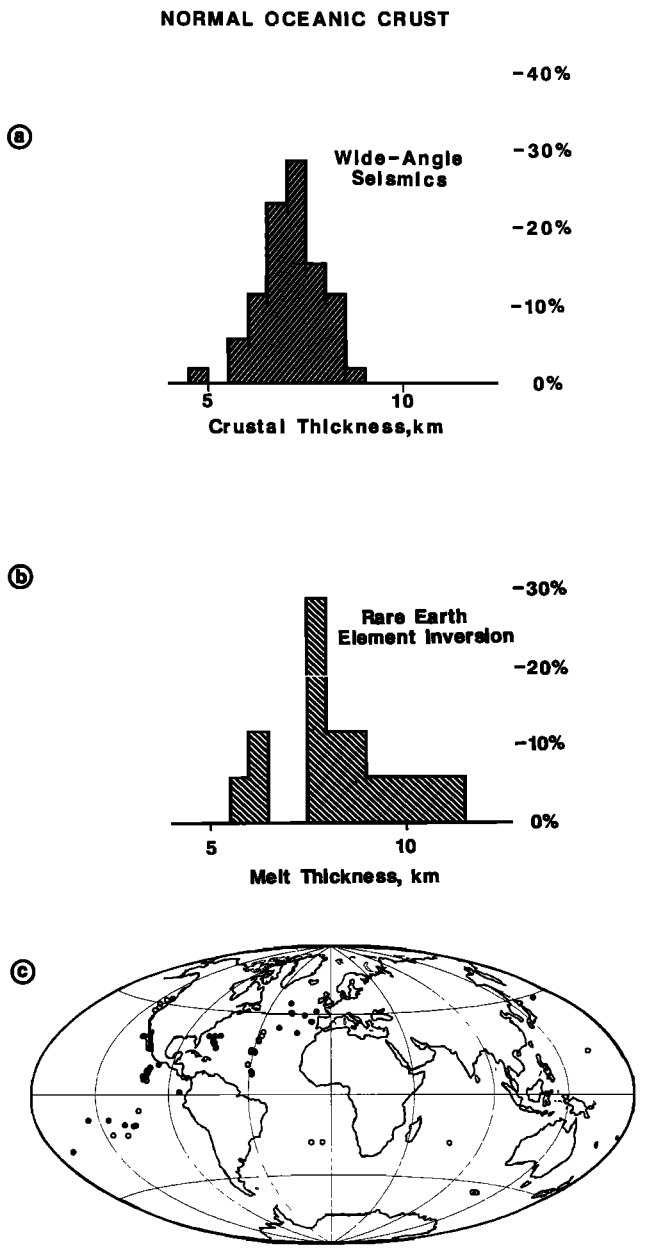

Fig. 10. Stacked curves of inferred melt distribution with depth for normal oceanic crust from suites R1–R17 in Figure 8. The heavy dotted line shows the melt distribution calculated using the expressions of *McKenzie and Bickle* [1988], but with ΔS = 400 J/(kg °C) and with allowance for compaction of the residue as melt is extracted. Melting stops at an equivalent depth of 7 km and produces a melt thickness of 8.3 km (the average calculated from the rare earth inversions of normal MORB) when T_p = 1330 °C.

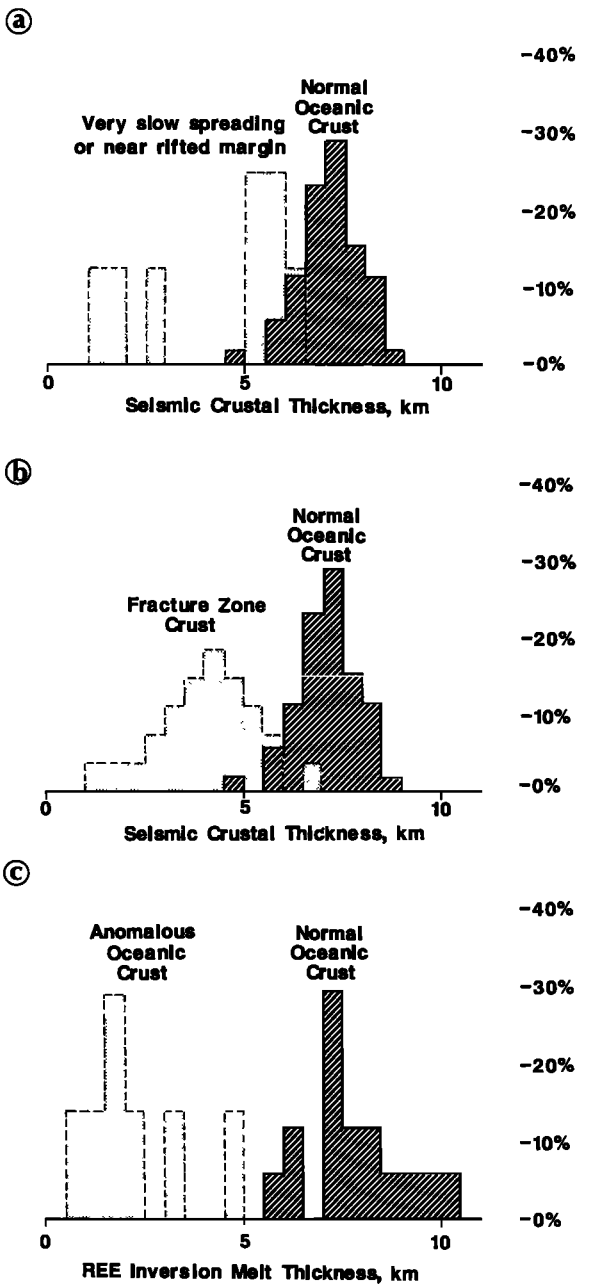

Fig. 11. Histograms of (a) seismic crustal thicknesses from very slow-spreading ridges and crust immediately adjacent to nonvolcanic rifted continental margins listed in Table 6 and compared with the thickness of normal oceanic crust from Table 4; (b) seismic crustal thicknesses from fracture zones listed in Table 6 and compared with the thickness of normal oceanic crust from Table 4; (c) inferred melt thicknesses from rare earth element inversions on basalts from anomalous crust found in fracture zones and on very slow-spreading ridges compared with inferred melt thicknesses from normal oceanic crust, both listed in Table 5.

McKenzie and Bickle's [1988] parameterization are significantly different from those observed for these small amounts of melt in anomalous oceanic crust. This difference may result from errors in the parameterization at small melt fractions. However, *Reid and Jackson*'s [1981] calculations suggest an alternative explanation. The calculated SiO_2 concentration is smaller, and that for MgO is greater, than is observed. These differences suggest that the melting zone is shallower than that calculated from the inversion scheme. For suite R23 from the south-west Indian Ridge we show in Appendix B the concentrations calculated using the melt distribution obtained from the inversion scheme, but with the top of the melting zone at the surface instead of at a depth of 40 km. The differences between the observed and calculated composition are then not significant for

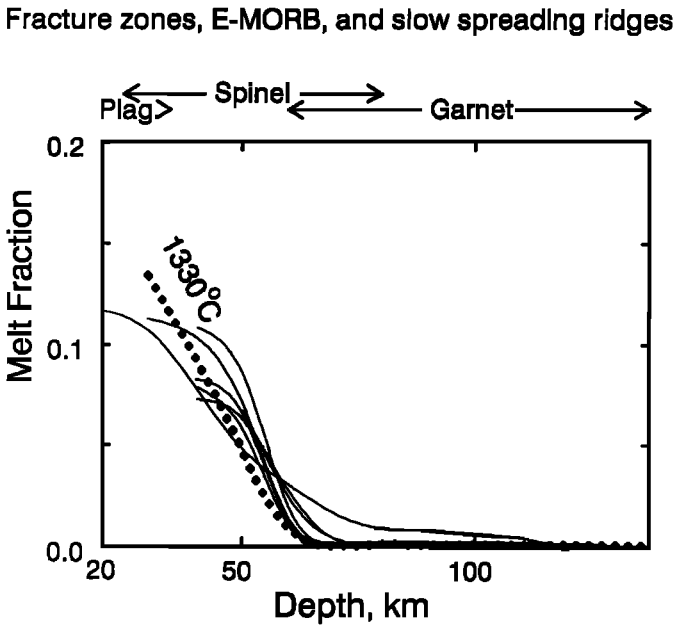

Fig. 12. Stacked curves of inferred melt distribution with depth for anomalous oceanic crust from suites R18–R24 in Figure 8. The heavy dotted line shows the melt distribution calculated using the expressions of *M^{c}Kenzie and Bickle* [1988], but with ΔS = 400 J/(kg °C) and with allowance for compaction of the residue as melt is extracted, for a potential temperature T_p = 1330 °C.

SiO_2 and MgO. This result suggests that the rare earth element concentrations are controlled by melting at the base of the melting zone, where melt is first generated within the upwelling mantle. *Reid and Jackson's* [1981] calculations show that little further melting occurs at shallower depths. If the melt from the base of the melting zone percolates upwards and remains in geochemical equilibrium with the matrix, the SiO_2 concentration will increase and that of MgO decrease. As shown in Appendix B, such a process can account for the observed major element concentrations.

Plume Affected Crust

Mantle plumes such as Hawaii, Iceland and the Cape Verdes generate a region of anomalously hot asthenospheric mantle which extends up to 1000 km away from the central plume [*Courtney and White*, 1986; *Watson and M^{c}Kenzie* , 1991]. When an oceanic spreading ridge cuts across such a thermal anomaly, greater quantities of melt than normal are generated by decompression melting of the mantle as it wells up beneath the spreading center [*M^{c}Kenzie and Bickle*, 1988; *White and M^{c}Kenzie* , 1989]. In the central core of the rising plume itself, considerable quantities of melt can be created, particularly where the lithosphere is very thin, as it is above Iceland.

Seismic results from spreading centers influenced by the Iceland mantle plume (Table 7 and Figure 13) show markedly thicker crustal sections than does normal oceanic crust. Because there is a paucity of good seismic data modeled using synthetic seismograms we have included in Table 7 six profiles modeled using modern travel time constraints: the scatter of these results is greater than those modeled using synthetic seismograms, which is not surprising in view of the greater uncertainty in the constraints on the Moho available from the tau-sum and ray-tracing methods which were applied. All the profiles, across a range of crustal ages, indicate that the crust formed at spreading centers above the thermal anomaly surrounding the Iceland mantle plume is thicker than normal (Figure 14*a*), with a mean of 10.3±1.7 km.

The geochemical samples used for rare earth element inversions (R25–R28, Figure 15), come from near the Azores, Iceland and Galapagos, all of which are associated with plumes that are now active, and from older sea floor near the Chagos-Laccadive Ridge, which is the trace of the Réunion plume. The distribution of enhanced melt thicknesses calculated from samples affected by plumes (Figure 14*b*) is very similar to the distribution obtained from seismic thickness determinations (Figure 14*a*). The mean crustal thickness calculated from the geochemical inversions is 10.7±1.6 km, in good agreement with the seismic results.

Melt Generated Within Plumes

Large quantities of melt are formed within the cores of mantle plumes, particularly when they lie beneath spreading centers and the melting region extends to shallow depths. Iceland lies directly above a rising mantle plume and is also intersected by the northern North Atlantic spreading ridge. This allows large quantities of melt to be generated since decompression of the convectively driven material in the mantle plume can continue to shallow levels as seafloor spreading continues. No seismic profiles across Iceland have been modeled with synthetic seismograms, although ray-tracing methods have been applied to the RRISP data [*Gebrande et al.*, 1980] and to some data shot across southern Iceland (Bjarnason et al., Tomographic image of the spreading center in southern Iceland, submitted to *Journal of Geophysical Research*, 1992). Large amplitude reflections from beneath southern Iceland reported by Bjarnason et al. are consistent with a Moho depth of 20–24 km, while on the RRISP profile further north the inferred crustal thickness is at least 30 km. Travel-time analysis of seismic profiles along the adjacent Iceland-Faeroe Ridge, where a normal Moho is developed, shows crustal thicknesses of 25–35 km [*Bott and Gunnarsson*, 1980].

There is evidence of similar large crustal thicknesses from other aseismic ridges formed above mantle plumes, but only two of these have been modeled with synthetics (Madagascar Ridge [*Sinha et al.*, 1981] and Kerguelen [*Recq et al.*, 1990]). The crustal thickness from seismic measurements controlled by synthetics averages

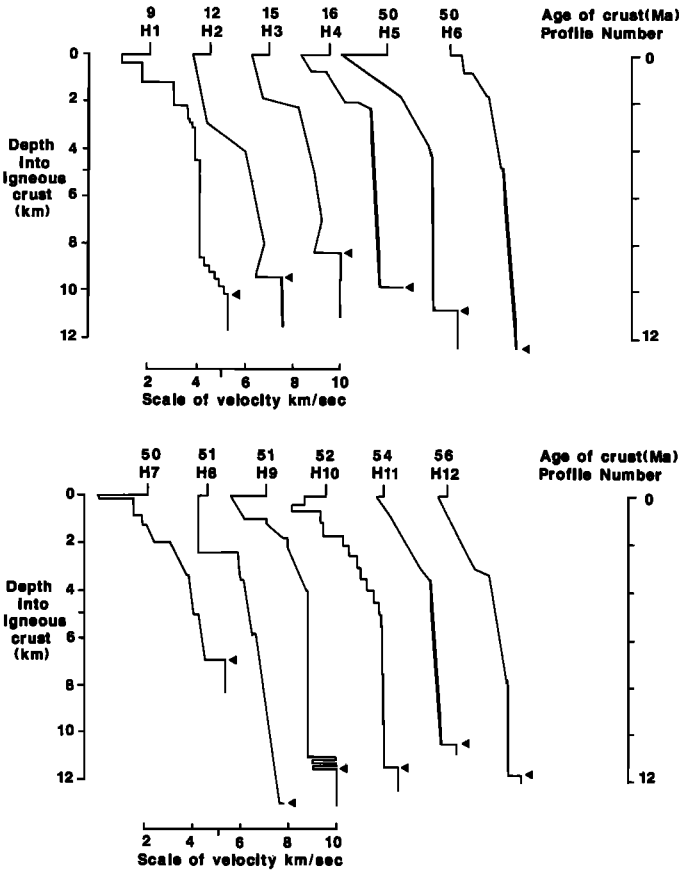

Fig. 13. Velocity-depth profiles of all available seismic profiles constrained by synthetic seismogram or modern travel time interpretations from oceanic crust formed at spreading centers in areas affected by the Iceland mantle plume, but not directly above the core of the plume. Sources are listed in Table 7. The profiles are aligned with zero depth at the top of the igneous basement. The horizontal scale of velocity is shown at the bottom of the figure, with the tick mark for each profile aligned at 5 km/s. Arrowhead on each profile shows location of the Moho.

20±1 km (Table 7 and Figure 16*a*). The larger sample of results modeled by slope – intercept methods suggests that the scatter of thicknesses from a range of plumes in different tectonic settings may be rather larger, although with a similar average thickness.

Geochemical analyses have been reported for basalts from Iceland [*O'Nions et al.*, 1976; *Grönvold*, 1973; *O'Nions and Grönvold*, 1973; *Nicholson and Latin*, 1992] and from the Ontong-Java plateau in the western Central Pacific [*Mahoney et al.*, 1992]. The residual depth anomalies in both areas are large and positive. The residual depth anomaly for Iceland is about 1 km greater than that for the Ontong-Java plateau, probably because there is still an active plume beneath Iceland that produces dynamic uplift of 1 km. Basalts from the Nauru basin and from the Cretaceous volcanics in the Central Pacific [*Floyd et al.*, 1991, 1992] are included in the 'plume' category on the basis of their composition, as *Saunders* [1985] has already argued. The mean crustal thickness from rare earth inversions is 17.8±0.6 km, similar to the seismic estimate.

Histograms of seismic thicknesses and melt thicknesses inferred from rare earth element inversions again show remarkably similar distributions (Figure 16). Inferred melt distributions with depth (Figure 17) show that melting starts much deeper than beneath normal mid-ocean ridges, a consequence of the higher mantle temperatures in the mantle plumes.

Discussion and Conclusions

The distributions of igneous crustal thickness measured using seismic techniques are strikingly similar to the inferred melt volumes calculated by inversion of rare earth element concentrations, across a wide variety of oceanic environments (Figures 9, 11, 14 and 16). This gives considerable confidence in our ability to use rare earth element distributions to investigate melting in the Earth and suggests that concentrations and standard deviations of the rare earth elements in the upper mantle used by *M'Kenzie and O'Nions* [1991] are correct.

Our compilation of seismic results from normal oceanic crust shows a mean crustal thickness of 7.1±0.8 km: this is greater than any previous compilations due to the improvements of synthetic seismogram modeling over earlier slope – intercept methods. Our

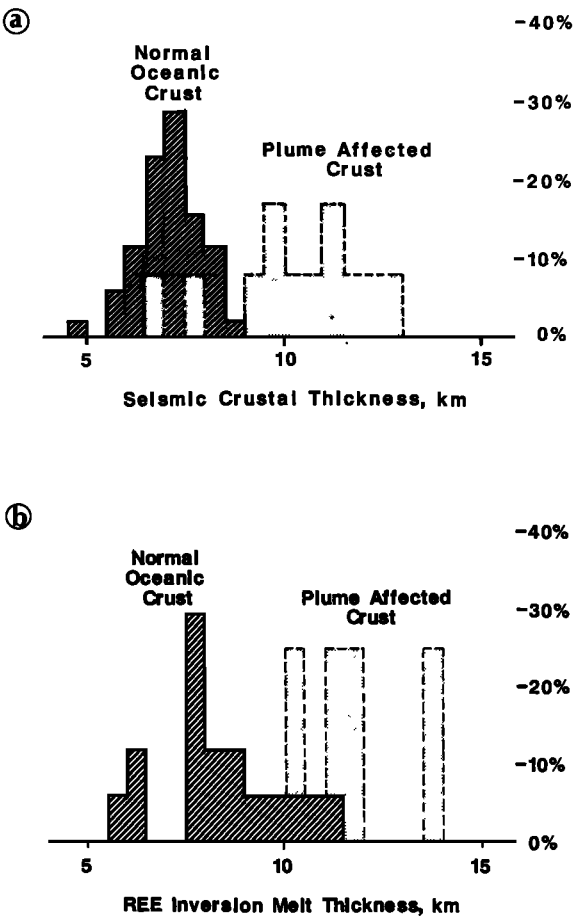

Fig. 14. Histograms of (a) seismic crustal thicknesses from spreading centers affected by the Iceland mantle plume listed in Table 7 and compared with the thickness of normal oceanic crust from Table 4; (b) inferred melt thicknesses from rare earth element inversions on basalts from crust affected by mantle plumes compared with inferred melt thicknesses from normal oceanic crust, both listed in Table 5.

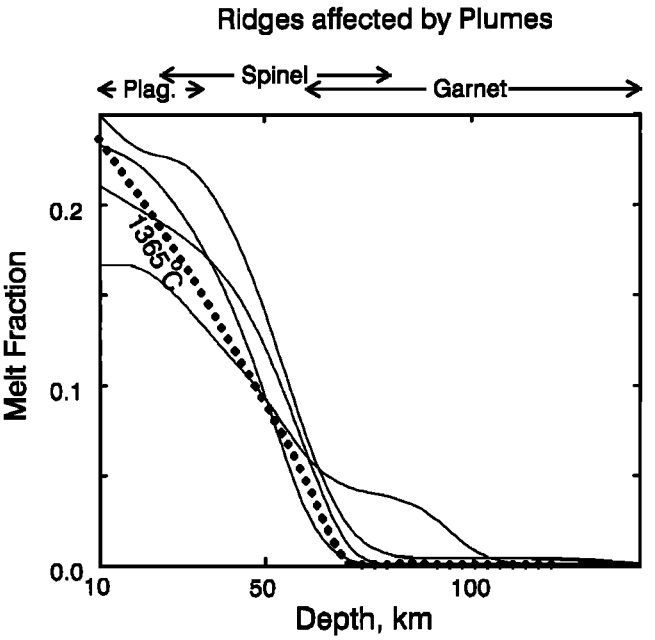

Fig. 15. Stacked curves of inferred melt distribution with depth for plume affected oceanic crust from suites R25–R28 in Figure 8. The heavy dotted line shows the melt distribution calculated using the expressions of *M^{c}Kenzie and Bickle* [1988], but with ΔS = 400 J/(kg °C) and with allowance for compaction of the residue as melt is extracted. A potential temperature T_p = 1365 °C produces 10.7 km of melt, the average calculated from the rare earth inversions.

results are consistent with systematic thickening of the ocean crust by 0.4–0.5 km over a 100 my period.

Inversion of rare earth element concentrations from seventeen independent suites of basalts produced by normal spreading ridges gives a mean melt thickness of 8.3±1.5 km. When the likely systematic errors are taken into account we do not believe that the difference between the igneous thicknesses inferred from seismic measurements and from geochemical inversions is significant. The major and minor element compositions calculated from *Watson and M^{c}Kenzie* 's [1991] parameterization agree well with those observed when olivine fractionation is taken into account.

The geochemical results are also in good agreement with *Klein and Langmuir*'s [1987] study of the Na concentrations in oceanic basalts. They argued that Na concentration increased as the melt volume, and therefore the crustal thickness, decreased. Though we did not include Na in the inversion calculations, its calculated mean concentration is compared in Appendix B with that observed. Except for anomalous crust, the difference between the two is not significant at the 95% level. In the case of anomalous crust the difference may result from failure of the major element parameterization at small melt fractions, where there are few experimental observations.

Results from ridges affected by plumes give similarly good agreement between the seismic thicknesses, which average 10.3±1.7 km and those from the inversions, which average 10.7±1.6 km. As in the case of normal MORB the calculated major and minor element compositions also agree well. When plumes coincide with spreading ridges larger amounts of melt are produced, though both the seismic and geochemical observations from such regions are still rather sparse. But the few crustal thickness estimates that exist are in good agreement, with the seismic measurements giving 20±1 km and the geochemical inversions 18±1 km.

It is striking that although seismic methods document marked local crustal thinning beneath fracture zones, the rare earth element inversions suggest that sometimes the degree of melt extraction which has generated the basalts in samples from fracture zones is the same as elsewhere. We suggest that melt may be intruded into the crust in focussed regions, but that it may then flow laterally along the ridge axis at crustal or surface levels. A mechanism of injection near segment centers and lateral flow was invoked by *White* [1984] to explain the gradual crustal thinning that is observed along the ridge axis as a fracture zone is approached, and the new rare earth element inversions provide support for this redistribution of melt.

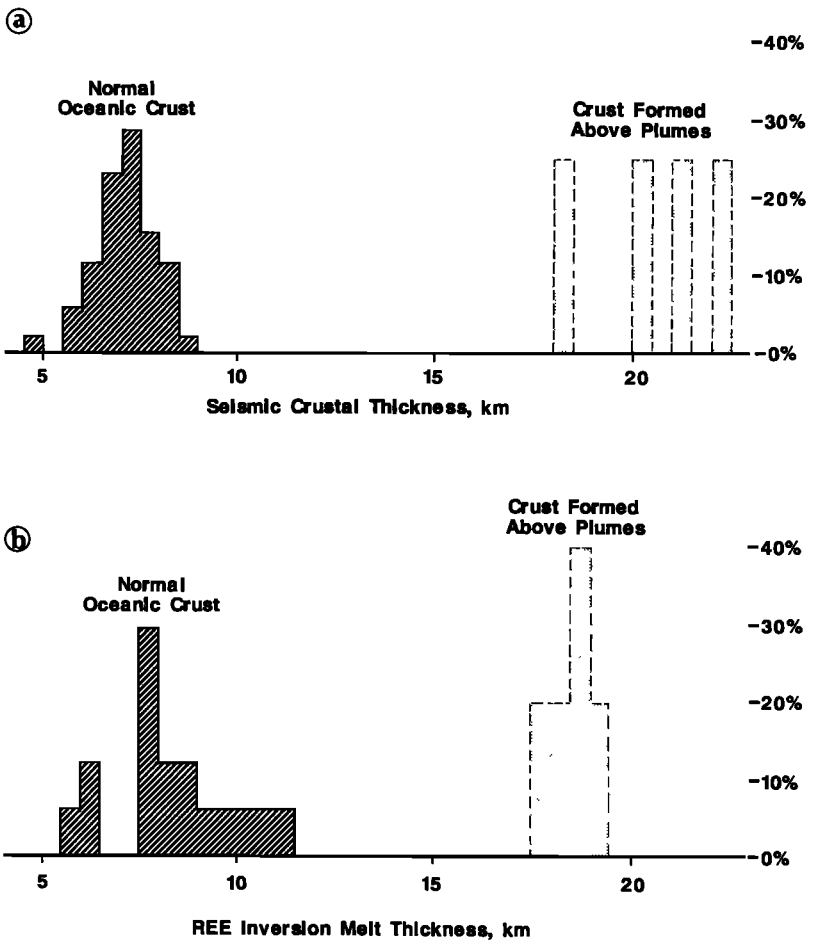

Fig. 16. Histograms of (a) seismic crustal thicknesses from aseismic ridges formed directly above mantle plumes listed in Table 7 and compared with the thickness of normal oceanic crust from Table 4; (b) inferred melt thicknesses from rare earth element inversions on basalts formed within mantle plumes compared with inferred melt thicknesses from normal oceanic crust, both listed in Table 5.

Further support for melt focusing in the mantle linked to the ridge segmentation comes from the apparent difference of ~0.5 km in crustal thickness between the Pacific and Atlantic seismic datasets (Table 8). The fast spreading Pacific has fracture zones only once every few hundred kilometers along the axis. By contrast, the slow spreading Atlantic exhibits fracture zones every 50–80 km along the axis. Our compilation of seismic results from normal Atlantic crust has specifically excluded fracture zone crust. If we compute the total crustal volume along a typical portion of Atlantic ridge axis, taking a mean segment length between fracture zones of 65 km and a mean thickness of 7 km, together with an average 10 km wide region of fracture zone crust which is only half the normal thickness, and then redistribute the crust as a uniform layer along the total 75 km length, we find an overall averaged crustal thickness of 6.5 km. This is 0.5 km less than the 'normal' Atlantic crustal thickness, and fits well with the observed difference between Atlantic and the thinner Pacific crust. This is evidence that the differences in apparent crustal thickness between normal segments of slow spreading Atlantic and fast spreading Pacific crust reflects the redistribution of melt beneath slow-spreading ridges. We conclude that for oceans formed at spreading rates above 20 mm/yr, this provides strong evidence that the same total amount of melt is produced under spreading centers regardless of spreading rate.

Such spreading rate independence is to be expected if the average mantle potential temperature is the same beneath all ridges, since the total volume of melt produced depends only on the initial entropy if heat loss by thermal conduction can be ignored. However, the melt production rate depends on the local upwelling rate of the mantle, which may well vary along ridge segments. This thermodynamic argument is only valid if all matrix velocities are upward beneath ridges: otherwise melt can be extracted from mantle which is then returned to the asthenosphere, and there are then no thermodynamic constraints on the total crustal thickness than can be produced.

At spreading rates below 20 mm/yr, both seismic measurements and rare earth inversions document a marked decrease in the amount of melt generated. This can be explained by conductive heat loss from the mantle beneath the spreading axes.

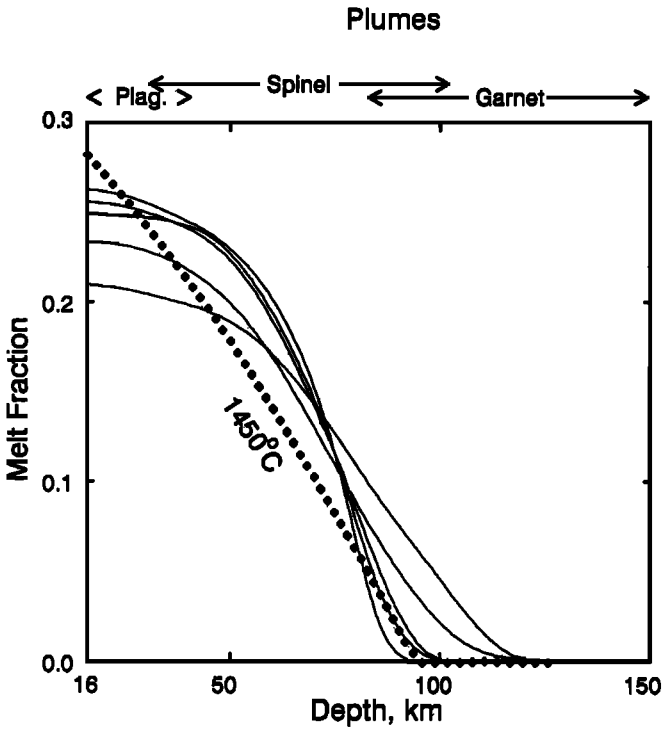

Fig. 17. Stacked curves of inferred melt distribution with depth for melt formed within plumes from suites R29–R33 in Figure 8. The heavy dotted lines show the melt distribution calculated using the expressions of *M^{c}Kenzie and Bickle* [1988], but with ΔS = 400 J/(kg °C) and with allowance for compaction of the residue as melt is extracted. A potential temperature T_p = 1450°C produces 18 km of melt, the same as the average of the rare earth element inversions.

It is surprising, and important, that the geochemical inversions give igneous thicknesses that are in such good agreement with those determined from seismology. The basalt samples from most of the ODP holes come from a few tens of meters of core below the sediment. Those from dredges are also from the top of the igneous crust. Therefore neither sampling method is likely to provide representative samples of average oceanic crust. Nonetheless the rare earth element concentrations are in excellent agreement with the seismic measurements that average the crustal thickness over distances of many tens of kilometers. Such agreement is unexpected. It suggests that the melt extraction process involves mixing of melts produced throughout the melting zone, and therefore provides an important constraint on melt separation beneath ridges. It also suggests that the geochemistry of fragments of oceanic crust that are common in orogenic belts can provide important information about the spreading ridges at which they were generated.

Appendix A

The principal difference between the inversion scheme used here and that of *M^{c}Kenzie and O'Nions* [1991] concerns the solution to the forward problem. *M^{c}Kenzie and O'Nions* [1991] used *Shaw's* [1970] analytic solution for fractional melting. His solution requires the bulk partition coefficient to remain constant throughout melt production (Figure A1*c*). This assumption is only satisfactory if phase changes do not occur in the matrix during the melting process. However, beneath ridges melting probably starts when garnet is still stable, and continues through the spinel stability field to depths where plagioclase is stable. All material will therefore start to melt in the presence of garnet, no matter what its present depth may be. Integration should therefore follow the melting path through the different stability fields (Figure A1*c*). A straightforward method of doing so uses the concentration in the residue c_s. Mass conservation requires

$$c_s(1 - X) + C_l X = \text{constant} \tag{1}$$

where X is the total melt fraction that has removed and C_l is the point average melt composition. Since

$$c_l = d(XC_l)/dX \tag{2}$$

where c_l is the instantaneous melt composition, differentiation of equation (1) gives

$$dc_s/dX = -(c_l - c_s)/(1 - X). \tag{3}$$

Shaw's [1970] expressions for $\overline{D}$ and $\overline{P}$ are then used to relate c_l and c_s

$$c_l = c_s(1 - X)/(\overline{D} - \overline{P}X). \tag{4}$$

The values of $\overline{D}$ and $\overline{P}$ were obtained from the values of D for the individual phases listed by *M^{c}Kenzie and O'Nions* [1991]. Because $\overline{D}$ and $\overline{P}$ are depth dependent, they are not constant on all integration paths. Equations (3) and (4) were integrated to obtain c_l and c_s using a fourth order Runge-Kutta scheme, starting with $X = 0$ at the base of the melting zone. If X decreased from a value X_{max} along the melting path, the total mass of each element in the solid was required to remain constant until X again exceeded X_{max}. Integration was stopped if $c_s(X)/c_s(0) \leq 10^{-4}$, and c_l set to zero for the remainder of the path. The point average and the point and depth average are easily calculated from $c_l(X)$ by integration.

Figure A1*a* compares the concentration ratios calculated using *Shaw's* [1970] expression with those using the path integral for the melt distribution obtained by *M^{c}Kenzie and O'Nions* [1991]. Because all paths start at the base of the melting zone, all parts of the zone generate their first 5% of melt in a region in which garnet is stable. The calculated heavy rare earth element concentrations are therefore lower. Melting occurs at shallower depths, and reaches larger melt fractions, when path integration, rather than *Shaw's* [1970] expression, is used for inversion (Figure A1*d*). However, the agreement between the observed and calculated ratios (Figure A1*b*) is similar for both cases. All inversions illustrated in

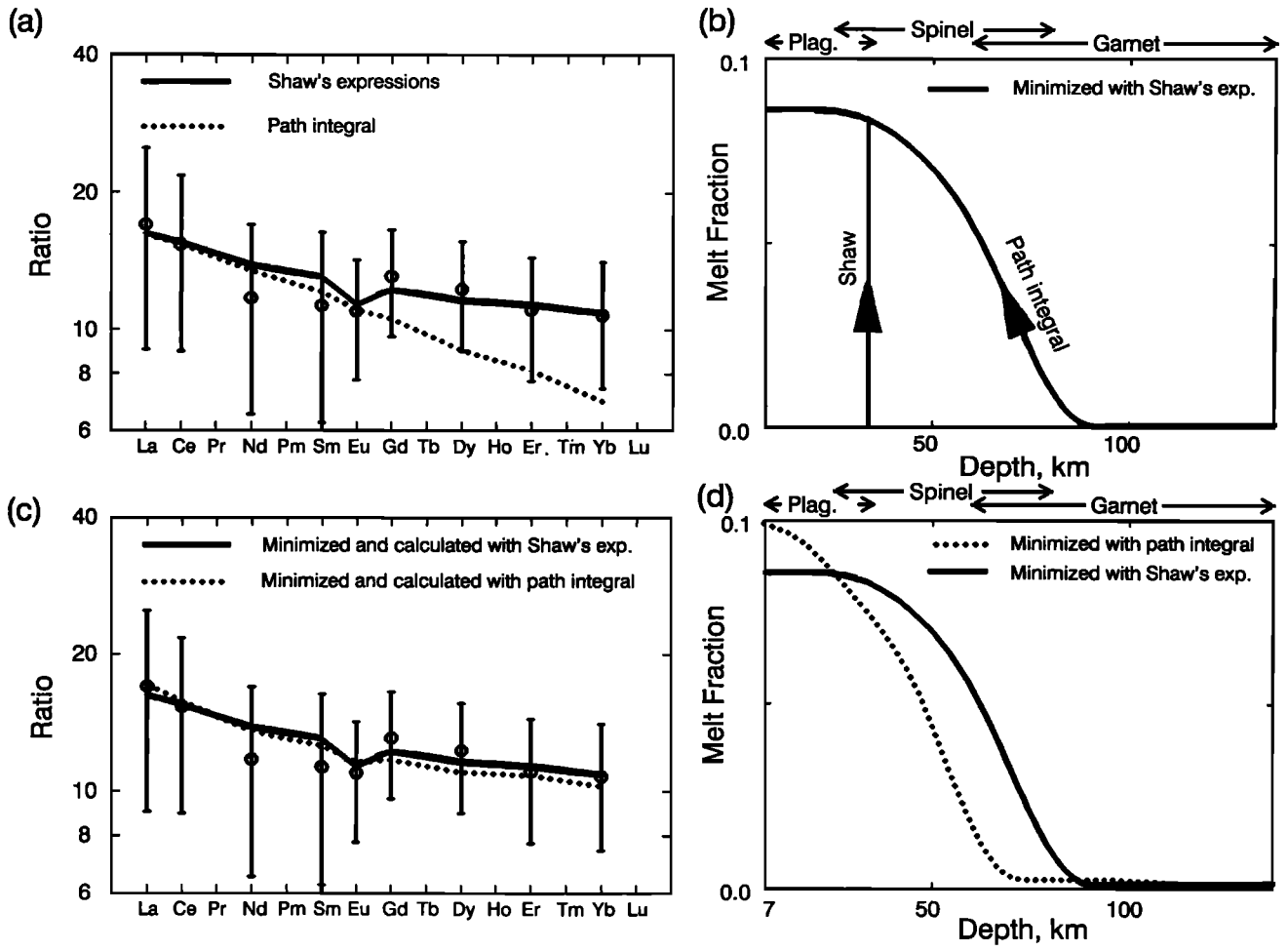

Fig. A1. *(a)* Rare earth element concentrations calculated using *Shaw's* [1970] expressions and the path integral method for the same melting model, shown in Figure A1*(b)*. *(c)* Comparison of the calculated concentration ratios from the best fitting melting model obtained using *Shaw's* [1970] expressions (solid line), and that from the path integral (dotted line). The two melt distributions are shown in *(d)*.

Appendix B were obtained using path integration, and with $W_3 = 0.1$, rather than 0.05, in equation (25) of *M'Kenzie and O'Nions* [1991].

One other modification was made to the calculations. *M'Kenzie and O'Nions* [1991] found the crustal thickness by evaluating

$$\int X dz \tag{5}$$

over the melting zone. This expression is not correct, because the present depth is measured within the residue, and not in the material before melting occurs. Equation (5) and other integrals over depth should be corrected for melt extraction, and then become

$$\int (X/(1-X))\, dz. \tag{6}$$

This correction increases the calculated crustal thickness. When X is small, as it is for MORB generation, the difference between equations (5) and (6) is small.

APPENDIX B

Table B1 compares the calculated and observed major and minor element concentrations, normalised to 100% with K_2O omitted. We only use samples with MgO $\geq$6% and with seven or more rare earth element concentrations.

Acknowledgments. We are grateful to T. Minshull for his comments on the compilation of seismic profiles, to J. Natland, G. Thompson, P. Castillo and J. Mahoney for their help in compiling the geochemical data and to Sharon Capon for drafting the velocity-depth profiles. This work forms part of projects investigating melt generation and the structure of oceanic basins, both of which are supported in part by the Natural Environment Research Council. Department of Earth Sciences contribution 2534.

REFERENCES

Bender, J. F., C. H. Langmuir, and G. N. Hanson, Petrogenesis of basalt glasses from the Tamayo region, East Pacific Rise, *J. Petrol., 25*, 213–254, 1984.

TABLE B1. Observed and Calculated Element Concentration Ratios

	SiO_2	TiO_2	Al_2O_3	FeO	MgO	CaO	Na_2O	K_2O
				Normal Oceanic Crust				
R1 (near Kane fracture zone, from *Bryan et al.* [1981])								
observed	50.5 ± 0.6	1.6 ± 0.3	15.9 ± 0.8	9.9 ± 0.8	7.9 ± 0.6	11.4 ± 0.6	2.8 ± 0.2	0.2 ± 0.0
calculated	49.9 ± 0.8	1.4 ± 0.2	15.8 ± 0.9	8.3 ± 1.0	10.6 ± 1.0	11.5 ± 1.1	2.5 ± 0.3	
rel. misfit[a]	0.6	0.6	0.0	1.3	-2.4	0.0	0.8	
R2 (holes 417A and 417D, western N Atlantic from *Shimizu et al.* [1980])								
observed	49.6 ± 0.8	1.5 ± 0.1	16.9 ± 0.3	9.8 ± 0.3	7.0 ± 0.4	12.7 ± 0.9	2.4 ± 0.2	0.1 ± 0.0
calculated	50.0 ± 0.8	1.3 ± 0.2	15.8 ± 0.9	8.2 ± 1.0	10.7 ± 1.0	11.6 ± 1.1	2.4 ± 0.3	
rel. misfit[a]	-0.4	1.0	1.1	1.6	-3.4	0.9	0.0	
R3 (Central Atlantic dredges from *Bougault et al.* [1988]; *Dosso et al.* [1991])								
observed	51.0 ± 0.3	1.6 ± 0.1	15.6 ± 0.9	9.8 ± 0.6	8.0 ± 0.6	11.5 ± 0.4	2.5 ± 0.3	0.2 ± 0.1
calculated	49.8 ± 0.8	1.5 ± 0.2	16.0 ± 0.9	8.2 ± 1.0	10.4 ± 1.0	11.5 ± 1.1	2.5 ± 0.3	
rel. misfit[a]	1.3	0.6	-0.3	1.4	-2.1	-0.1	-0.1	
R4 (hole 395A, Central Atlantic from *Rhodes et al.* [1979])								
observed	50.3 ± 0.5	1.5 ± 0.3	16.6 ± 1.4	9.4 ± 1.3	7.9 ± 0.6	11.6 ± 0.7	2.8 ± 0.1	0.2 ± 0.0
calculated	49.8 ± 0.8	1.4 ± 0.2	15.8 ± 0.9	8.3 ± 1.0	10.7 ± 1.0	11.5 ± 1.1	2.4 ± 0.3	
rel. misfit[a]	0.5	0.4	0.5	0.7	-2.5	0.1	1.1	
R5 (hole 519B, South Atlantic from *Dietrich et al.* [1984])								
observed	50.9 ± 0.3	1.2 ± 0.1	15.7 ± 0.4	8.7 ± 0.2	8.8 ± 0.3	12.5 ± 0.0	2.2 ± 0.1	0.0 ± 0.0
calculated	50.1 ± 0.8	1.1 ± 0.2	15.5 ± 0.9	8.4 ± 1.0	11.2 ± 1.0	11.4 ± 1.1	2.2 ± 0.3	
rel. misfit[a]	0.9	0.4	0.2	0.3	-2.3	1.0	-0.2	
R6 (hole 522B South Atlantic from *Dietrich et al.* [1984])								
observed	51.4 ± 0.4	1.5 ± 0.1	15.4 ± 0.2	9.0 ± 0.5	7.8 ± 0.2	12.4 ± 0.3	2.5 ± 0.1	0.1 ± 0.1
calculated	50.0 ± 0.8	1.3 ± 0.2	15.7 ± 0.9	8.3 ± 1.0	10.8 ± 1.0	11.5 ± 1.1	2.4 ± 0.3	
rel. misfit[a]	1.5	0.8	-0.3	0.6	-2.9	0.8	0.2	
R7 (Mid Atlantic Ridge and East Pacific Rise from *Sun et al.* [1979]; *Johnson* [1979]; *Kay et al.* [1970])								
observed	50.2 ± 0.9	1.5 ± 0.5	16.0 ± 1.7	10.5 ± 1.9	7.6 ± 1.2	11.7 ± 0.8	2.6 ± 0.2	0.2 ± 0.1
calculated	49.9 ± 0.8	1.4 ± 0.2	16.0 ± 0.9	8.2 ± 1.0	10.5 ± 1.0	11.5 ± 1.1	2.5 ± 0.3	
rel. misfit[a]	0.2	0.2	0.0	1.1	-1.8	0.1	0.4	
R8 (dredged samples, East Pacific Rise from *Thompson et al.* [1989])								
observed	51.0 ± 0.3	1.9 ± 0.2	15.0 ± 0.6	10.6 ± 0.8	7.0 ± 0.4	11.6 ± 0.6	2.9 ± 0.1	0.2 ± 0.1
calculated	49.6 ± 0.8	1.6 ± 0.2	16.0 ± 0.9	8.3 ± 1.0	10.4 ± 1.0	11.5 ± 1.1	2.6 ± 0.3	
rel. misfit[a]	1.6	1.0	-0.9	1.8	-3.1	0.1	1.0	
R9 (dredged samples, East Pacific Rise near Tamayo fracture zone from *Bender et al.* [1984])								
observed	49.9 ± 0.3	1.2 ± 0.1	15.8 ± 0.4	9.4 ± 0.2	8.9 ± 0.5	12.5 ± 0.3	2.2 ± 0.2	0.0 ± 0.0
calculated	50.1 ± 0.8	1.2 ± 0.2	15.7 ± 0.9	8.2 ± 1.0	10.8 ± 1.0	11.5 ± 1.1	2.3 ± 0.3	
rel. misfit[a]	-0.2	0.1	0.1	1.1	-1.6	0.9	-0.3	
R10 (holes 428 and 429A, East Pacific Rise from *Srivastava et al.* [1980])								
observed	51.4 ± 0.6	1.6 ± 0.1	15.2 ± 0.6	10.0 ± 0.7	7.6 ± 0.3	11.7 ± 0.4	2.6 ± 0.1	0.2 ± 0.1
calculated	50.4 ± 0.8	1.0 ± 0.2	15.4 ± 0.9	8.3 ± 1.0	11.2 ± 1.0	11.5 ± 1.1	2.2 ± 0.3	
rel. misfit[a]	0.9	1.9	-0.3	1.4	-3.4	0.2	1.5	
R11 (holes 482B and 483, Mouth of Gulf of California from *Saunders* [1983])								
observed	50.2 ± 0.8	1.7 ± 0.4	15.4 ± 0.6	10.2 ± 1.2	7.8 ± 0.6	12.0 ± 0.6	2.6 ± 0.2	0.1 ± 0.1
calculated	49.8 ± 0.8	1.5 ± 0.2	16.1 ± 0.9	8.2 ± 1.0	10.4 ± 1.0	11.6 ± 1.1	2.6 ± 0.3	
rel. misfit[a]	0.4	0.2	-0.6	2.1	-2.6	0.4	0.1	
R12 (holes 597B and 599B, Eastern Pacific from *Pearce et al.* [1986])								
observed	50.9 ± 0.4	1.2 ± 0.2	15.0 ± 0.9	10.3 ± 1.0	7.8 ± 0.4	12.3 ± 0.5	2.4 ± 0.3	0.1 ± 0.1
calculated	50.1 ± 0.8	1.2 ± 0.2	15.8 ± 0.9	8.2 ± 1.0	10.7 ± 1.0	11.5 ± 1.1	2.4 ± 0.3	
rel. misfit[a]	0.8	0.0	-0.6	1.5	-2.7	0.6	0.1	
R13 (hole 504B, Costa Rica Rift from *Emmermann* [1985])								
observed	50.3 ± 1.6	1.0 ± 0.3	16.2 ± 0.8	8.8 ± 1.0	9.1 ± 0.7	12.6 ± 0.7	2.1 ± 0.2	0.0 ± 0.0
calculated	49.9 ± 0.8	1.1 ± 0.2	15.4 ± 0.9	8.6 ± 1.0	11.5 ± 1.0	11.4 ± 1.1	2.2 ± 0.3	
rel. misfit[a]	0.1	-0.3	0.6	0.2	-1.8	0.9	-0.2	

TABLE B1. (continued)

	SiO_2	TiO_2	Al_2O_3	FeO	MgO	CaO	Na_2O	K_2O
				Normal Oceanic Crust (continued)				
R14 (hole 504B, Costa Rica Rift from *Tual et al.* [1985])								
observed	50.0 ± 1.4	1.1 ± 0.2	16.0 ± 0.9	9.4 ± 0.8	8.6 ± 0.8	13.1 ± 0.4	1.8 ± 0.4	0.1 ± 0.1
calculated	50.2 ± 0.8	1.1 ± 0.2	15.5 ± 0.9	8.3 ± 1.0	11.2 ± 1.0	11.5 ± 1.1	2.2 ± 0.3	
rel. misfit[a]	-0.1	-0.1	0.4	0.9	-2.0	1.5	-0.8	
R15 (hole 801C, Pigafetta Basin, Pacific from *Floyd et al.* [1992])								
observed	49.7 ± 1.1	1.8 ± 0.3	14.7 ± 1.2	11.5 ± 1.4	7.1 ± 0.5	12.4 ± 0.5	2.8 ± 0.2	0.1 ± 0.1
calculated	50.0 ± 0.8	1.4 ± 0.2	16.0 ± 0.9	8.1 ± 1.0	10.4 ± 1.0	11.6 ± 1.1	2.5 ± 0.3	
rel. misfit[a]	-0.3	1.0	-0.8	2.0	-2.9	0.7	0.8	
R16 (dredged samples, South East Indian Ridge from *Klein et al.* [1991])								
observed	50.8 ± 0.8	1.2 ± 0.1	16.3 ± 0.6	8.4 ± 0.4	8.8 ± 0.4	11.5 ± 0.3	3.0 ± 0.2	0.1 ± 0.0
calculated	49.8 ± 0.8	1.3 ± 0.2	15.5 ± 0.9	8.6 ± 1.0	11.2 ± 1.0	11.4 ± 1.1	2.4 ± 0.3	
rel. misfit[a]	0.9	-0.2	0.7	-0.2	-2.1	0.2	1.8	
R17 (dredged samples from the South East and Central Indian Ridges from *Price et al.* [1986])								
observed	51.3 ± 0.1	1.3 ± 0.2	15.8 ± 0.5	8.8 ± 0.6	8.4 ± 0.3	11.4 ± 0.3	3.0 ± 0.1	0.1 ± 0.0
calculated	50.0 ± 0.8	1.3 ± 0.2	15.7 ± 0.9	8.4 ± 1.0	10.8 ± 1.0	11.5 ± 1.1	2.4 ± 0.3	
rel. misfit[a]	1.6	0.0	0.1	0.4	-2.3	0.0	1.9	
				Anomalous Oceanic Crust				
R18 (dredged samples from Tamayo fracture zone *Bender et al.* [1984])								
observed	49.7 ± 0.4	1.8 ± 0.3	15.2 ± 0.7	10.6 ± 0.7	8.1 ± 0.6	12.0 ± 0.4	2.7 ± 0.2	0.1 ± 0.0
calculated	48.4 ± 0.8	1.5 ± 0.2	16.0 ± 0.9	8.8 ± 1.0	11.3 ± 1.0	11.5 ± 1.1	2.6 ± 0.3	
rel. misfit[a]	1.5	0.8	-0.7	1.4	-2.7	0.5	0.3	
R19 (hole 427, Siqueiros fracture zone from *Srivastava et al.* [1980])								
observed	51.0 ± 0.4	2.6 ± 0.0	14.0 ± 0.1	12.7 ± 0.2	6.7 ± 0.2	10.0 ± 0.2	3.0 ± 0.1	0.1 ± 0.0
calculated	47.8 ± 0.8	1.7 ± 0.2	16.1 ± 0.9	9.1 ± 1.0	11.3 ± 1.0	11.5 ± 1.1	2.7 ± 0.3	
rel. misfit[a]	3.6	3.8	-2.2	3.7	-4.5	-1.4	1.1	
R20 (Atlantis II fracture zone, E. side, from *Johnson and Dick* [in press, 1992])								
observed	51.4 ± 0.5	2.1 ± 0.2	15.4 ± 0.5	10.5 ± 0.6	6.8 ± 0.4	10.3 ± 0.4	3.4 ± 0.2	0.2 ± 0.0
calculated	47.8 ± 0.8	1.6 ± 0.2	15.9 ± 0.9	9.1 ± 1.0	11.4 ± 1.0	11.4 ± 1.1	2.6 ± 0.3	
rel. misfit[a]	3.8	1.3	-0.5	1.2	-4.3	-1.0	2.2	
R21 (Atlantis II fracture zone, W. side, from *Johnson and Dick* [1992])								
observed	50.7 ± 0.4	1.9 ± 0.3	15.3 ± 0.6	10.6 ± 0.8	7.6 ± 0.6	10.8 ± 0.5	3.1 ± 0.2	0.1 ± 0.0
calculated	47.9 ± 0.8	1.5 ± 0.2	15.8 ± 0.9	9.2 ± 1.0	11.6 ± 1.0	11.4 ± 1.1	2.6 ± 0.3	
rel. misfit[a]	3.0	1.0	-0.4	1.1	-3.5	-0.5	1.7	
R22 (dredged E-type MORB, East Pacific Rise from *Thompson et al.* [1989])								
observed	51.0 ± 0.3	2.2 ± 0.0	16.0 ± 0.5	10.0 ± 0.2	6.6 ± 0.2	11.0 ± 0.3	3.3 ± 0.0	0.7 ± 0.0
calculated	48.0 ± 0.8	1.7 ± 0.2	15.1 ± 0.9	9.7 ± 1.0	12.0 ± 1.0	10.9 ± 1.1	2.6 ± 0.3	
rel. misfit[a]	3.5	1.8	0.8	0.4	-5.4	0.1	2.4	
R23 (dredged samples from S W Indian Ridge near Rodriguez triple junction from *Price et al.* [1986])								
observed	51.0 ± 0.4	1.2 ± 0.3	17.4 ± 0.2	7.8 ± 0.1	8.4 ± 0.8	10.4 ± 0.3	3.8 ± 0.2	0.2 ± 0.0
calc., top at 40 km	49.0 ± 0.8	1.4 ± 0.2	15.5 ± 0.9	8.9 ± 1.0	11.4 ± 1.0	11.3 ± 1.1	2.4 ± 0.3	
rel. misfit[a]	2.2	-0.4	2.0	-1.1	-2.4	-0.8	3.6	
calc., top at 0 km	50.9 ± 0.8	1.4 ± 0.2	15.9 ± 0.9	7.8 ± 1.0	10.0 ± 1.0	11.5 ± 1.1	2.5 ± 0.3	
rel. misfit[a]	0.1	-0.5	1.6	0.0	-1.2	-1.0	3.5	
R24 (dredged samples from the Mid-Cayman Rise from *Thompson et al.* [1980]; *Thompson, personal communication, 1991*)								
observed	51.9 ± 0.6	1.8 ± 0.3	16.1 ± 0.5	9.2 ± 0.7	7.1 ± 0.5	10.3 ± 0.4	3.6 ± 0.2	0.2 ± 0.0
calculated	47.9 ± 0.8	1.6 ± 0.2	15.7 ± 0.9	9.3 ± 1.0	11.6 ± 1.0	11.3 ± 1.1	2.6 ± 0.3	
rel. misfit[a]	4.1	0.7	0.3	-0.1	-4.0	-0.9	3.0	
				Plume Affected Oceanic Crust				
R25 (holes 411, 412A and 413 near the Azores islands from *Wood et al.* [1979])								
observed	49.8 ± 1.6	0.8 ± 0.2	16.2 ± 1.2	8.6 ± 0.5	9.8 ± 3.5	12.6 ± 0.7	2.2 ± 0.4	0.1 ± 0.1
calculated	49.8 ± 0.8	1.0 ± 0.2	15.2 ± 0.9	8.6 ± 1.0	11.9 ± 1.0	11.4 ± 1.1	2.1 ± 0.3	
rel. misfit[a]	0.0	-0.4	0.7	0.0	-0.6	0.9	0.2	

TABLE B1. (continued)

	SiO_2	TiO_2	Al_2O_3	FeO	MgO	CaO	Na_2O	K_2O
R26 (holes 407, 408 and 409 South of Iceland from *Wood et al.* [1979])								
observed	50.4 ± 0.8	1.8 ± 0.6	14.3 ± 0.6	11.5 ± 1.5	7.9 ± 1.0	11.8 ± 0.4	2.4 ± 0.1	0.2 ± 0.1
calculated	49.5 ± 0.8	1.4 ± 0.2	15.5 ± 0.9	8.7 ± 1.0	11.1 ± 1.0	11.3 ± 1.1	2.5 ± 0.3	
rel. misfit[a]	0.8	0.6	-1.1	1.5	-2.4	0.4	-0.3	
R27 (Galapagos Rift: hole 425 from *Srivastava et al.* [1980]; holes 506G, 507B, 510 from *Emmermann et al.* [1983])								
observed	50.9 ± 0.3	1.1 ± 0.4	14.9 ± 1.0	10.3 ± 1.8	7.9 ± 0.8	12.7 ± 1.3	2.2 ± 0.2	0.0 ± 0.0
calculated	49.7 ± 0.8	1.2 ± 0.2	15.6 ± 0.9	8.5 ± 1.0	11.2 ± 1.0	11.5 ± 1.1	2.3 ± 0.3	
rel. misfit[a]	1.4	-0.2	-0.5	0.9	-2.6	0.8	-0.5	
R28 (holes 220, 221, and 236, near Chagos-Laccadive Ridge from *Frey et al.* [1980])								
observed	51.9 ± 0.8	1.1 ± 0.3	15.0 ± 1.5	11.7 ± 1.2	7.5 ± 0.6	10.5 ± 0.9	2.2 ± 0.4	0.3 ± 0.2
calculated	49.7 ± 0.8	1.2 ± 0.2	15.6 ± 0.9	8.6 ± 1.0	11.3 ± 1.0	11.4 ± 1.1	2.3 ± 0.3	
rel. misfit[a]	2.0	-0.2	-0.3	2.1	-3.3	-0.6	-0.2	
Melt Generated Within Plumes								
R29 (Iceland basalts from *O'Nions et al.* [1976]; *Grönvold* [1973]; *O'Nions and Grönvold* [1973])								
observed	49.4 ± 1.3	1.2 ± 0.3	14.3 ± 0.9	11.5 ± 1.3	8.9 ± 1.9	12.6 ± 0.8	2.0 ± 0.3	0.1 ± 0.1
calculated	48.9 ± 0.8	1.2 ± 0.2	14.6 ± 0.9	9.5 ± 1.0	12.7 ± 1.0	10.9 ± 1.1	2.2 ± 0.3	
rel. misfit[a]	0.3	0.1	- 0.2	1.2	-1.8	1.2	-0.4	
R30 (Krafla basalts from *Nicholson and Latin* [1992])								
observed	49.3 ± 0.7	1.2 ± 0.4	15.4 ± 0.4	10.6 ± 0.8	9.0 ± 0.5	12.8 ± 0.7	1.9 ± 0.2	0.1 ± 0.0
calculated	49.0 ± 0.8	1.1 ± 0.2	14.7 ± 0.9	9.4 ± 1.0	12.8 ± 1.0	11.0 ± 1.1	2.1 ± 0.3	
rel. misfit[a]	0.3	0.2	0.6	1.0	-3.4	1.4	-0.8	
R31 (hole 462A, Nauru Basin from *Saunders* [1985])								
observed	50.6 ± 0.7	1.3 ± 0.4	14.5 ± 0.4	11.8 ± 0.8	7.4 ± 0.4	11.9 ± 0.7	2.3 ± 0.2	0.1 ± 0.0
calculated	49.0 ± 0.8	1.1 ± 0.2	15.0 ± 0.9	9.2 ± 1.0	12.4 ± 1.0	11.1 ± 1.1	2.2 ± 0.3	
rel. misfit[a]	1.5	0.5	-0.4	2.1	-4.5	0.6	0.2	
R32 (hole 802A into Cretaceous volcanics, Mariana Basin from *Floyd et al.* [1992])								
observed	51.1 ± 0.6	1.2 ± 0.0	14.8 ± 0.2	11.0 ± 0.5	7.8 ± 0.2	12.0 ± 0.2	2.1 ± 0.1	0.1 ± 0.1
calculated	49.0 ± 0.8	1.0 ± 0.2	14.8 ± 0.9	9.3 ± 1.0	12.7 ± 1.0	11.1 ± 1.1	2.1 ± 0.3	
rel. misfit[a]	2.1	0.7	-0.1	1.6	-4.7	0.8	0.1	
R33 (holes 803 and 807, Ontong-Java Plateau from *Mahoney et al.* [1992])								
observed	50.4 ± 0.6	1.3 ± 0.2	14.6 ± 0.4	11.6 ± 0.9	7.4 ± 0.6	12.4 ± 0.3	2.3 ± 0.2	0.2 ± 0.1
calculated	49.0 ± 0.8	1.1 ± 0.2	14.9 ± 0.9	9.2 ± 1.0	12.5 ± 1.0	11.1 ± 1.1	2.2 ± 0.3	
rel. misfit[a]	1.4	0.7	-0.3	1.8	-4.3	1.1	0.4	
Anomalous MORB From Normal Ridge Axis								
R34 (Central Atlantic dredges near 14°N from *Bougault et al.* [1988])								
observed	51.2 ± 1.6	1.4 ± 0.3	15.4 ± 0.4	9.6 ± 0.5	8.4 ± 1.5	11.4 ± 0.7	2.5 ± 0.4	0.5 ± 0.1
calculated	49.4 ± 0.8	1.4 ± 0.2	14.9 ± 0.9	9.2 ± 1.0	11.8 ± 1.0	10.9 ± 1.1	2.4 ± 0.3	
rel. misfit[a]	1.1	0.1	0.5	0.3	-1.9	0.4	0.2	

[a]relative misfit is [(observed-calculated)/standard deviation] for each element.

Bott, M. H. P., and K. Gunnarson, Crustal structure of the Iceland-Faeroe Ridge, *J. Geophys., 47*, 221–227, 1980.

Bougault, H., L. Dmitriev, J.-G. Schilling, A. Sobolev, J.-L. Joron, and H. D. Needham, Mantle heterogeneity from trace elements: MAR triple junction near 14°N, *Earth Planet. Sci. Lett., 88*, 27–36, 1988.

Bratt, S. R., and G. M. Purdy, Structure and variability of oceanic crust on the flanks of the East Pacific Rise between 11° and 13°N, *J. Geophys. Res., 89*, 6111–6125, 1984.

Bratt, S. R., and S. C. Solomon, Compressional and shear wave structure of the East Pacific Rise at 11°20′N: Constraints from three-component ocean bottom seismometer data, *J. Geophys. Res., 89*, 6095–6110, 1984.

Bryan, W. B., G. Thompson, and J. N. Ludden, Compositional variation in normal MORB from 22°N–25°N: Mid-Atlantic Ridge and Kane fracture zone, *J. Geophys. Res., 86*, 11815–11836, 1981.

Bunch, A. W. H., and B. L. N. Kennett, The crustal structure of the Reykjanes Ridge at 59°30′N, *Geophys. J. R. Astron. Soc., 61*, 141–166, 1980.

Cary, P. W., and C. H. Chapman, Waveform inversion of Expanding Spread Profile 5 from the North Atlantic Transect, *J. Geophys. Res., 93*, 13,575–13,588, 1988.

Christensen, N. I., and M. H. Salisbury, Structure and composition of the lower oceanic crust, *Rev. Geophys., 13*, 57–86, 1975.

Collins, J. A., G. M. Purdy, and T. M. Brocher, Seismic velocity structure at Deep Sea Drilling Project Site 504B, Panama Basin: Evidence for thin oceanic crust, *J. Geophys. Res., 94*, 9283–9302, 1989.

Cormier, M.-H., R. S. Detrick, and G. M. Purdy, Anomalously thin crust in oceanic fracture zones: New seismic constraints from the Kane fracture zone, *J. Geophys. Res., 89*, 10,249–10,266, 1984.

Courtney, R. C., and R. S. White, Anomalous heat flow and geoid across the Cape Verde Rise: evidence for dynamic support from a thermal plume in the mantle, *Geophys. J. R. Astron. Soc., 87*, 815–868, plus microfiche GH 87/1, 1986.

Detrick, R. S. Jr., and G. M. Purdy, The crustal structure of the Kane fracture zone from seismic refraction studies, *J. Geophys. Res, 85*, 3759–3777, 1980.

Detrick, R. S., M.-H. Cormier, R. A. Prince, D. W. Forsyth, and E. L. Ambos, Seismic constraints on the crustal structure within the Vema fracture zone, *J. Geophys. Res., 87*, 10,599–10,612, 1982.

Dietrich, V. J., M. F. Carman, A. Wyttenbach, and E. H. McKee, Geochemistry of basalts from holes 519A, 520, 522B and 524, *Initial Rep. Deep Sea Drill. Proj., 73*, 579–601, 1984.

Dosso, L., B. B. Hanan, H. Bougault, J.-G. Schilling, and J.-L. Joron, Sr-Nd-Pb geochemical morphology between 10° and 17°N on the Mid-Atlantic Ridge: A new MORB isotope signature, *Earth Planet. Sci. Lett., 106*, 29–43, 1991.

Duennebier, F. K., B. Lienert, R. Cessaro, P. Anderson, and S. Mallick, Controlled-source seismic experiment at Hole 581C, *Initial Rep. Deep Sea Drill. Proj., 88*, 105–125, 1987.

Emmerman, E., Basement geochemistry, hole 504B, *Initial Rep. Deep Sea Drill. Proj., 83*, 183–200, 1985.

Emmermann R., H.-W. Hubberten, and H. Puchelt, Geochemistry of basalts erupted at the Galapagos spreading center between 85 and 87°W, *Initial Rep. Deep Sea Drill. Proj., 70*, 409–418, 1983.

Floyd, P. A., P. R. Castillo, and M. Pringle, Tholeiitic and alkalic basalts of the oldest Pacific Ocean crust, *Terra Nova, 3*, 257–265, 1991.

Floyd, P. A., J. A. Winchester, and P. R. Castillo, Geochemistry and petrography of Cretaceous sills and lava flows, sites 800 and 802, *Proc. Ocean Drill. Program, Sci. Results, 129*, in press, 1992.

Fowler, C. M. R., Crustal structure of the Mid-Atlantic ridge crest at 37°N, *Geophys. J. R. Astron. Soc., 47*, 459–492, 1976.

Fowler, C. M. R., The mid-Atlantic ridge: Structure at 45°N, *Geophys. J. R. Astron. Soc., 54*, 167–183, 1978.

Fowler, C. M. R., and C. E. Keen, Oceanic crustal structure – Mid-Atlantic Ridge at 45°N, *Geophys. J. R. Astron. Soc., 56*, 219–226, 1979.

Fowler, S. R., R. S. White, G. D. Spence, and G. K. Westbrook, The Hatton Bank continental margin, II, Deep structure from two-ship expanding spread seismic profiles, *Geophys. J., 96*, 295–309, 1989.

Frey, F. A., J. S. Dickey, G. Thompson, W. B. Bryan, and H. L. Davies, Evidence for heterogeneous primary MORB and mantle sources, N W Indian Ocean, *Contrib. Mineral. Petrol., 74*, 387–402, 1980.

Gebrande, H., H. Miller, and P. Einarrson, Seismic structure of Iceland along RRISP–Profile I, *J. Geophys., 47*, 239–249, 1980.

Ginzburg, A., R. B. Whitmarsh, D. G. Roberts, L. Montadert, A. Camus, and F. Avedik, The deep seismic structure of the northern continental margin of the Bay of Biscay, *Ann. Geophys., 3*, 499–510, 1985.

Goslin, J., P. Bauzart, J. Francheteau, and X. Le Pichon, Thickening of the oceanic layer in the Pacific Ocean, *Mar. Geophys. Res, 1*, 418–427, 1972.

Grönvold, K., Structural and petrochemical studies in the Kerlingarfjöll region, central Iceland, Ph.D. dissertation, Univ. of Oxford, Oxford, England, 1973.

Hayes, D. E., Age-depth relationships and depth anomalies in the southeast Indian Ocean and South Atlantic Ocean, *J. Geophys. Res., 93*, 2937–2954, 1988.

Helmberger, D. V., and G. Engen, Fine structure of an oceanic crustal section near the East Pacific Rise, *Bull. Seismol. Soc. Am., 68*, 369–382, 1978.

Helmberger, D. V., and G. B. Morris, A travel time and amplitude interpretation of a marine refraction profile: Transformed shear waves, *Bull. Seismol. Soc. Am., 60*, 593–600, 1970.

Hill, M. N., Recent geophysical exploration of the ocean floor, *Progr. Phys. Chem. Earth, 2*, 129–163, 1957.

Horsefield, S. J., Crustal structure across the continent-ocean boundary, Ph.D. dissertation, Univ. of Cambridge, Cambridge, England, 1992.

Horsefield, S. J., R. B. Whitmarsh, R. S. White, and J.-C. Sibuet, Crustal structure of the Goban Spur passive continental margin, North Atlantic - Results of a detailed seismic refraction survey, *Geophys. J. Int.*, in press, 1992.

Houtz, R. E., Crustal structure of the North Atlantic on the basis of large-airgun—sonobuoy data, *Geol. Soc. Am. Bull., 91*, 406–413, 1980.

Jackson, H. R., I. Reid, and R. K. H. Falconer, Crustal structure near the Arctic mid-ocean ridge, *J. Geophys. Res., 87*, 1773–1783, 1982.

Johnson, J. R., Transitional basalts and tholeiites from the East Pacific Rise, 9°N, *J. Geophys. Res., 84*, 1635–1652, 1979.

Johnson, K. T. M., and H. J. B. Dick, Open system melting and temporal and spatial variation of peridotite and basalt at the Atlantis II fracture zone, *J. Geophys. Res., 97*, 9219–9241, 1992.

Kay, R., N. J. Hubbard, and P. W. Gast, Chemical characteristics and origins of oceanic ridge volcanics, *J. Geophys. Res., 75*, 1585–1613, 1970.

Keen, M. J., R. Courtney, J. McClain, and G. M. Purdy, Ocean-ridge crustal thickness correlated with paleobathymetry (abstract), *EOS Trans. AGU, 71*, 1573, 1990.

Keen, C., and C. Tramontini, A seismic refraction survey on the Mid-Atlantic Ridge, *Geophys. J. R. Astron. Soc., 20*, 473–491, 1970.

Kennett, B. L. N., and J. A. Orcutt, A comparison of travel time inversions for marine refraction profiles, *J. Geophys. Res., 81*, 4061–4070, 1976.

Klein, E. M., and C. H. Langmuir, Global correlations of ocean ridge basalt chemistry with axial depth and crustal thickness, *J. Geophys. Res., 92*, 8089–8115, 1987.

Klein, E. M., C. H. Langmuir, and H. Staudigel, Geochemistry of basalts from the southeast Indian Ridge, 115°E–138°E, *J. Geophys. Res., 96*, 2089–2107, 1991.

Larsen, H. C., and S. Jakobsdóttir, Distribution, crustal properties and significance of seaward dipping subbasement reflectors off east Greenland, in Early Tertiary Volcanism and the Opening of the NE Atlantic, edited by A. C. Morton and L. M. Parson, *Geol. Soc. London Spec. Publ., 39*, 95–114, 1988.

Le Douran, S., and B. Parsons, A note on the correction of ocean floor depths for sediment loading, *J. Geophys. Res., 87*, 4715–4722, 1982.

Le Pichon, X., R. E. Houtz, C. L. Drake, and E. Nafe, Crustal structure of the mid-ocean ridges, 1, Seismic refraction measurements, *J. Geophys. Res., 70*, 319–340, 1965.

Lewis, B. T. R., and J. D. Garmany, Constraints on the structure of the East Pacific Rise from seismic refraction data, *J. Geophys. Res., 87*, 8417–8425, 1982.

Lewis, B. T. R., and W. E. Snydsman, Fine structure of the lower oceanic crust on the Cocos Plate, *Tectonophysics, 55*, 87–105, 1979.

Lindwall, D. A., Old Pacific crust near Hawaii: A seismic view, *J. Geophys. Res., 96*, 8191–8203, 1991.

Louden, K. E., R. S. White, C. G. Potts, and D. W. Forsyth, Structure and seismotectonics of the Vema fracture zone, Atlantic Ocean, *J. Geol. Soc. London, 143*, 795–805, 1986.

Mahoney, J. J., M. Storey, R. A. Duncan, K. J. Spencer, and M. Pringle, Geochemistry and geochronology of the Ontong Java Plateau, *Proc. Ocean Drill. Program, Sci. Results, 130*, in press, 1992.

McClain, J. S., On long-term thickening of the oceanic crust, *Geophys. Res. Lett., 8*, 1191–1194, 1981.

McClain, J. S., and C. A. Atallah, Thickening of the oceanic crust with age, *Geology, 14*, 574–576, 1986.

McKenzie, D., and M. J. Bickle, The volume and composition of melt generated by extension of the lithosphere, *J. Petrol., 29*, 625–679, 1988.

McKenzie, D., and R. K. O'Nions, Partial melt distributions from inversion of rare earth element concentrations, *J. Petrol., 32*, 1021–1091, 1991 (Correction, *J. Petrol., 33*, in press, 1992.)

McKenzie, D., and R. K. O'Nions, Correction to *Partial melt distributions from inversion of rare earth element concentrations*, *J. Petrol., 33*, in press, 1992.

Minshull, T. A., R. S. White, J. C. Mutter, P. Buhl, R. S. Detrick, C. A. Williams, and E. Morris, Crustal structure at the Blake Spur fracture zone from expanding spread profiles, *J. Geophys. Res., 96*, 9955–9984, 1991.

Mithal, R., and J. C. Mutter, A low-velocity zone within the layer 3 region of 118 Myr old oceanic crust in the western North Atlantic: *Geophys. J., 97*, 275–294, 1989.

Morgan, J. V., P. J. Barton, and R. S. White, The Hatton Bank continental margin, III, Structure from wide-angle OBS and multichannel seismic refraction profiles, *Geophys. J. Int., 98*, 367–384, 1989.

Morris, E., R. S. Detrick, T. A. Minshull, J. C. Mutter, R. S. White, W. Su, and P. Buhl, Seismic structure of oceanic crust in the western North Atlantic, *J. Geophys. Res.*, in press, 1992.

Mutter, J. C., and C. M. Zehnder, Deep crustal structure and magmatic processes: the inception of seafloor spreading in the Norwegian–Greenland Sea, in Early Tertiary Volcanism and the Opening of the NE Atlantic, edited by A. C Morton, and L. M. Parson, *Geol. Soc. London Spec. Publ., 39*, 35–48, 1988.

Nicholson, H., and D. Latin, Olivine tholeiites from Krafla, Iceland: Evidence for variations in melt fraction within a plume, *J. Petrol.*, in press, 1992.

Olafsson, I., E. Sundvor, O. Eldholm, and K. Grue, Møre margin: Crustal structure from analysis of expanded spread profiles, *Marine Geophys. Res., 14*, 137–162, 1992.

O'Nions, R. K., and K. Grönvold, Petrogenic relationships of acid and basic rocks in Iceland: Sr-isotopes and rare-earth elements in late and postglacial volcanics, *Earth Planet. Sci. Lett., 19*, 397–409, 1973.

O'Nions, R. K., R. J. Pankhurst, and K. Grönvold, Nature and development of basalt magma sources beneath Iceland and the Reykjanes Ridge, *J. Petrol., 17*, 315–338, 1976.

Orcutt, J. A., B. L. N. Kennett, and L. M. Dorman, Structure of the East Pacific Rise from an ocean bottom seismometer survey, *Geophys. J. R. Astron. Soc., 45*, 305–320, 1976.

Parsons, B., and J. G. Sclater, An analysis of the variation of ocean floor bathymetry and heat flow with age, *J. Geophys. Res., 82*, 803–827, 1977.

Pearce, J. A., N. Rogers, A. J. Tindle, and J. S. Watson, Geochemistry and petrogenesis of basalts from Deep Sea Drilling Project Leg 92, eastern Pacific, *Initial Rep. Deep Sea Drill. Proj., 92*, 435–457, 1986.

Pinheiro, L. M., R. B. Whitmarsh, and P. R. Miles, The ocean-continent boundary off the western continental margin of Iberia, part II, Crustal structure in the Tagus Abyssal Plain, *Geophys. J. Int., 109*, 106–124, 1992.

Potts, C. G., R. S. White, and K. E. Louden, Crustal structure of Atlantic fracture zones, II, The Vema fracture zone and transverse ridge, *Geophys. J. R. Astron. Soc., 86*, 491–513, 1986*a*.

Potts, C. G., A. J. Calvert, and R. S. White, Crustal structure of Atlantic fracture zones, III, The Tydeman fracture zone, *Geophys. J. R. Astron. Soc., 86*, 909–942, 1986*b*.

Price, R. C., A. K. Kennedy, M. Riggs-Sneeringer, and F. A. Frey. Geochemistry of basalts from the Indian Ocean triple junction: Implications for the generation and evolution of Indian Ocean ridge basalts, *Earth Planet. Sci. Lett., 78*, 379–396, 1986.

Purdy, G. M., The seismic structure of 140 Myr old crust in the western central Atlantic Ocean, *Geophys. J. R. Astron. Soc., 72*, 115–137, 1983.

Purdy, G. M., and R. S. Detrick, Crustal structure of the Mid-Atlantic Ridge at 23°N from seismic refraction studies, *J. Geophys. Res., 91*, 3739–3762, 1986.

Purdy, G. M., New observations of the shallow seismic structure of young oceanic crust, *J. Geophys. Res., 92*, 9351–9362, 1987.

Raitt, R. W., Seismic refraction studies of the Pacific Ocean basin, *Geol. Soc. Am. Bull., 67*, 1623–1640, 1956.

Raitt, R. W., The crustal rocks, in *The Sea*, vol. 3, edited by M. N. Hill, pp. 85–102, Wiley-Interscience, New York, 1963.

Recq, M., D. Brefort, J. Malod, and J.-L. Veinante, The Kerguelen Isles (southern Indian Ocean): New results on deep structure from refraction profiles, *Tectonophysics, 182*, 227–248, 1990.

Reid, I., and H. R. Jackson, Oceanic spreading rate and crustal thickness, *Mar. Geophys. Res., 5*, 165–172, 1981.

Renkin, M. L., and J. G. Sclater, Depth and age in the North Pacific, *J. Geophys. Res., 93*, 2919–2935, 1988.

Rhodes, J. M., D. P. Blanchard, M. A. Dungan, K. V. Rodgers, and J. C. Brannon, Chemistry of Leg 45 basalts, *Initial Rep. Deep Sea Drill. Proj., 45*, 447–459, 1979.

Ritzert, M., and W. R. Jacoby, On the lithospheric seismic structure of Reykjanes Ridge at 62.5°N, *J. Geophys. Res., 90*, 10,117–10,128, 1985.

Saunders, A. D., Geochemistry of basalts recovered from the Gulf of California during Leg 65 of the Deep Sea Drilling Project, *Initial Rep. Deep Sea Drill. Proj., 65*, 591–621, 1983.

Saunders, A. D., Geochemistry of basalts from the Nauru basin, Deep Sea Drilling Project legs 61 and 89: Implications for the origin of oceanic flood basalts, *Initial Rep. Deep Sea Drill. Proj., 89*, 499–517, 1985.

Searle, R. C., and R. B. Whitmarsh, The structure of King's Trough, northeast Atlantic, from bathymetric, seismic and gravity studies, *Geophys. J. R. Astron. Soc., 53*, 259–288, 1978.

Shaw, D. M., Trace element fractionation during anatexis, *Geochim. Cosmochim. Acta, 34*, 237–243, 1970.

Shearer, P. M., and J. A. Orcutt, Compressional and shear wave anisotropy in the oceanic lithosphere – The Ngendei seismic refraction experiment, *Geophys. J. R. Astron. Soc., 87*, 967–1004, 1986.

Shimizu, H., A. Masuda, and T. Vi, Determination of rare-earth elements in leg 51, site 417 samples, *Initial Rep. Deep Sea Drill. Proj., 51, 52, 53, Part 2*, 1113–1120, 1980.

Shor, G. G. Jr., H. W. Menard, and R. S. Raitt, Structure of the Pacific Basin, in *The Sea*, vol. 4, Part II, edited by A. E. Maxwell, pp. 3–27, Wiley-Interscience, New York, 1970.

Sinha, M. C., and K. E. Louden, The Oceanographer Fracture Zone, I, Crustal Structure from seismic refraction studies, *Geophys. J. R. Astron. Soc., 75*, 713–736, 1983.

Sinha, M. C., K. E. Louden, and B. Parsons, The crustal structure of the Madagascar Ridge, *Geophys. J. R. Astron. Soc., 66*, 351–377, 1981.

Spence, G. D., R. S. White, G. K. Westbrook, and S. R. Fowler, The Hatton Bank continental margin, I, Shallow structure from two-ship expanding spread seismic profiles, *Geophys. J., 96*, 273–294, 1989.

Spudich, P. A., Oceanic crustal studies using waveform analysis and shear waves, Ph.D. Dissertation, 125 pp., Univ. of Calif., San Diego, 1979.

Spudich, P., and J. Orcutt, A new look at the seismic velocity structure of the oceanic crust, *Rev. Geophys., 18*, 627–645, 1980*a*.

Spudich, P., and J. Orcutt, Petrology and porosity of an oceanic site: results from wave form modeling of seismic refraction data, *J. Geophys. Res., 85*, 1409–1433, 1980*b*.

Srivastava, R. K., R. Emmermann, and H. Puchelt, Petrology and geochemistry of basalts from Deep Sea Drilling Project Leg 54, *Initial Rep. Deep Sea Drill. Proj., 54*, 671–693, 1980.

Sun, S.-S., R. N. Nesbitt, and A. Ya. Sharaskin, Geochemical characteristics of Mid-Ocean Ridge basalts, *Earth Planet. Sci. Lett., 44*, 119–138, 1979.

Thompson, G., W. B. Bryan, and W. G. Melson, Geological and geophysical investigation of the Mid-Cayman Rise spreading center: geochemical variation and petrogenesis of basalt glasses, *J. Geol., 88*, 41–55, 1980.

Thompson, G., W. B. Bryan, and S. E. Humphris, Axial volcanism on the East Pacific Rise, 10-12°N, in Magmatism in the Ocean Basins, edited by A. D. Saunders and M. J. Norry, *Geol. Soc. London Spec. Publ., 42*, 181–200, 1989.

Tréhu, A., and G. M. Purdy, Crustal structure in the Orozco transform zone, *J. Geophys. Res., 89*, 1834–1842, 1984.

Tual, E., B. M. John, H. Bougault, and J. L. Joron, Geochemistry of basalts from hole 504B, leg 83, Costa Rica Rift, *Initial Rep. Deep Sea Drill. Proj., 83*, 201–214, 1985.

Vera, E. E., P. Buhl, J. C. Mutter, A. J. Harding, J. A. Orcutt, and R. S. Detrick, The structure of 0–0.2 m.y. old oceanic crust at 9°N in the East Pacific Rise from expanded spread profiles, *J. Geophys. Res., 95*, 15,529–15,556, 1990.

Waldron, D. A., R. M. Clowes, and D. J. White, Seismic structure of a subducting oceanic plate off western Canada, in Studies of Laterally Heterogenous Structures Using Seismic Refraction and Reflection Data, edited by A. G. Green, *Pap. Geol. Surv. Can., 89-13*, 105–113, 1990.

Watson, S., and D. McKenzie, Melt generation by plumes: A study of Hawaiian volcanism, *J. Petrol., 32*, 501–537, 1991.

White, R. S., Oceanic upper crustal structure from variable angle seismic reflection-refraction profiles, *Geophys. J. R. Astron. Soc., 57*, 683–726, 1979.

White, R. S., Atlantic oceanic crust: seismic structure of a slow spreading ridge, in Ophiolites and Oceanic lithosphere, edited by I. G. Gass, S. J. Lippard and A. W. Shelton, pp. 101–111, Geological Society London, 1984.

White, R. S., The Earth's crust and lithosphere, in Oceanic and Continental Lithosphere: Similarities and Differences, edited by M. A. Menzies and K. Cox, *J. Petrol. Spec. Lithosphere Issue*, 1–10, 1988.

White, R. S., Crustal structure and magmatism of North Atlantic continental margins, *J. Geol. Soc. London, 149*, in press, 1992.

White, R. S., and D. H. Matthews, Variations in oceanic upper crustal structure in a small area of the northeastern Atlantic, *Geophys. J. R. Astron. Soc., 61*, 401–431, 1980.

White, R. S., and D. P. McKenzie, Magmatism at rift zones: The generation of volcanic continental margins and flood basalts, *J. Geophys. Res., 94*, 7685–7729, 1989.

White, R. S., R. S. Detrick, M. C. Sinha, and M. H. Cornier, Anomalous seismic crustal structure of oceanic fracture zones, *Geophys. J. R. Astron. Soc., 79*, 779–798, 1984.

White, R. S., R. S. Detrick, J. Mutter, P. Buhl, T. A. Minshull, and E. Morris, New seismic images of oceanic crustal structure, *Geology, 18*, 462–465, 1990.

Whitmarsh, R. B., Seismic refraction studies of the upper igneous crust in the North Atlantic and porosity estimates for Layer 2, *Earth Planet. Sci. Lett., 37*, 451–464, 1978.

Whitmarsh, R. B., and A. J. Calvert, Crustal structure of Atlantic Fracture Zones, I, The Charlie Gibbs F. Z., *Geophys. J. R. Astron. Soc., 85*, 107–138, 1986.

Whitmarsh, R. B., A. Ginzburg, and R. C. Searle, The structure and origin of the Azores-Biscay Rise, north-east Atlantic Ocean, *Geophys. J. R. Astron. Soc., 70*, 79–108, 1982.

Whitmarsh, R. B., P. R. Miles, and A. Mauffret, The ocean-continent boundary off the western continental margin of Iberia, I, Crustal structure at 40°30′N, *Geophys. J. Int., 103*, 509–531, 1990.

Wood, D. A., J. Tarney, J. Varet, A. D. Saunders, H. Bougault, J. L. Joron, M. Treuil, and J. R. Cann, Geochemistry of basalts drilled in the North Atlantic by IPOD leg 49: Implications for mantle heterogeneity, *Earth Planet. Sci. Lett., 42*, 77–97, 1979.

Woollard, G. P., The inter-relationships of crustal and upper mantle parameter values in the Pacific, *Rev. Geophys., 13*, 87–137, 1975.

D. P. McKenzie and R. S. White, Bullard Laboratories, Cambridge University, Madingley Road, Cambridge CB3 OEZ, England.

R. K. O'Nions, Department of Earth Sciences, Cambridge University, Downing Street, Cambridge CB2 3EQ, England.

(Received December 27, 1991;
revised July 10, 1992;
accepted July 20, 1992.)